PARAMETRIC AMPLIFICATION IN MEMS DEVICES

CHEO KOON LIN
(B.Eng. (Hons.), NUS)

A THESIS SUBMITTED

FOR THE DEGREE OF MASTER OF ENGINEERING

DEPARTMENT OF MECHANICAL ENGINEERING

NATIONAL UNIVERSITY OF SINGAPORE

2003

Acknowledgements

This project would have been impossible if not for the contributions of many people. First of all I would like to thank A/P Francis Tay Eng Hock. This project would not have even taken off if not for his enthusiasm in allowing me to attempt something akin to stepping off into the unknown. His undying support was truly heartening to a student who had almost lost all hope in making sense of the world of MEMs.

To A/P Chau Fook Siong for accommodating all the blunders that were made along the way. His earnest comments were invaluable every step of the way. My heartfelt appreciation to Mr. Logeeswaran, our Research Engineer in MEMsLab. All the discussions and help he offered were simply priceless. His passion for research simply rubs off everyone in the lab, making it an enjoyable experience simply to be even there. To YeeYuan, who never fails to amaze me with his breadth of knowledge. The discussions with him over electronics were indispensable. It would have been impossible for a mechanical engineer to make sense of the various aspects of electrical engineering on his own. To Meilin for sharing all the secrets of detection schemes. To Jyh Siong, for all the discussions we had. Many thanks to Prof C.H. Ling and Mdm Lian Kiat at MOS lab in ECE, for their tolerance of an intruder to their MMR vacuum probe. To everyone else who had helped in one way or another.

And finally to my family for their understanding of why I hadn’t been home.

Table Of Contents

Summary

Parametric amplification in a low capacitance MEMS parallel-plate device is demonstrated. The behaviour of such small capacitance devices is shown to still follow theoretical approximations. The general power gain of such a system is shown to be dependent on load and capacitance change, γ_n. A means of estimating characterization of capacitance change of the device at resonance (γ_n) through the extraction from current parameters is proposed.

γ_1 values ranging from 0.001 to 0.008 are obtained, which limits the effective gain and characteristics of the parametric amplifier. However, as the device used was an improvised gyroscope, the resonant frequency of ~1800 Hz and γ_1 are not as high as would have liked. Theoretical values predicted insufficient gain and are confirmed through experiment.

A new resonance detection scheme is proposed, which removes the necessity for a DC-bias to the device. The resonance characteristics of this *3f*-detection scheme are analysed and demonstrated. The simplicity and elegance of this scheme made possible the detection of resonance for one-port devices with high parasitic capacitance. Previous known methods were limited to 2-port devices only.

An Electrical Equivalent Modelling scheme is also proposed, based on Bond Graph modelling. It allows the representation of mechanical systems in electrical domain, a convenient methodology in MEMS. Though not a suitable method for parametric devices, it is also suggested how mechanical parameters can be extracted from electrical signals. Some future modifications will be required for appropriate application.

List of Figures

List of Tables

List of Symbols

ε	Permittivity of vacuum, 8.854×10^{-12} F/m
h	Planck's constant, 6.626×10^{-34} Js
k	Boltzmann's constant, 1.3807×10^{-23} JK^{-1}
L	Inductance
C	Capacitance
R	Resistance
Q	Charge
Z	Impedance
V	Voltage
I	Current
k	Spring Constant
m	mass
c	damping coefficient
P	Power
w	frequency
γ_n	capacitance ratio, $\frac{C_n}{2C_0}$

CHAPTER 1: Introduction

1.1 Background

The theory of parametric amplification is not new. The foundation of such amplification systems had been laid since Manley and Rowe's paper in 1956 [1], [2]. However, the relevance of such devices has changed with time. In the 1960s, great interest was generated in such amplification in the search for low-noise amplification. The advent of the maser ("microwave amplification by stimulated emission") satisfied the noise requirements for microwave engineers. The aim then was to obtain a means of achieving the low-noise properties of the maser but yet retain the simplicity in application of a transistor. That was a time when the semiconductor transistor was in its infant phase. Thus there was a need for the pursuit of parametric amplifiers because it offered the theoretical possibility of amplification at a low level of background noise. The relevance is noted in transmission systems where the level of external noise is low, the main source of noise being the receiver's intrinsic noise sources (e.g. space telecommunication). The first implementation of such parametric amplifiers used semiconductor varactors as the non-linear capacitance device. [3].

With progress in the understanding and design of low-noise transistor circuits, parametric amplification lost flavour. Moreover, early designs for microwave parametric amplifiers were cumbersome and complex in implementation. An early design by Philips Corporation [28] is shown in Fig. 1.1.

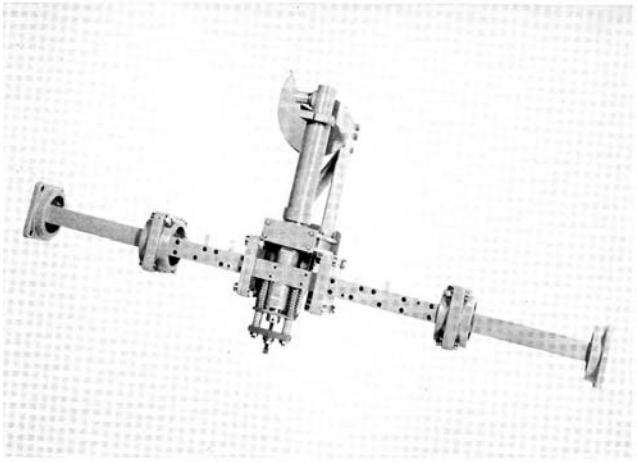

Fig. 1.1. Microwave parametric amplifier operating at 9480 MHz

However, such schemes still continued to be actively researched and implemented in optical transmission techniques today. An example is an optical parametric amplification (OPA) system. It is a nonlinear interaction in which two light waves of frequencies w_1 and w_2 are amplified in a medium which is

irradiated with an intense pump wave of frequency w_3. [4][5].

1.2. Noise and Reactance

How then does a parametric amplifier obtain low noise levels? It will first be necessary to understand the mechanisms of noise. In simple terms, Nyquist [6] showed that the thermal noise power from a conductor at the physical temperature, T (K) is

$$N = N_{\Delta f} = \frac{hf}{e^{\frac{hf}{kT}} - 1} \Delta f \ \text{[W]} \qquad 1.1$$

where $h = 6.626 \times 10^{-34} Js$ is Planck's constant, $k = 1.3807 \times 10^{-23} JK^{-1}$ is Boltzmann's constant, f is the frequency and Δf is the bandwidth of the measuring system, both in Hz. For hf << kT, a condition which is satisfied at room temperature for frequencies less than a comfortable 600 GHz, this is reduced to

$$N = kT\Delta f \ \text{[W]} \qquad 1.2$$

The noise power model for a one-port resistance is then given by the stochastic expression

$$N = \frac{\left\langle |e|^2 \right\rangle}{4R} \ \text{[W]} \qquad 1.3$$

where R is the resistance value of the element.

In simple terms, resistive elements are attributed to be the main source of thermal noise. Amplification circuits today rely on semiconductors, which add shot noise [7] to the system.

Reactance is an element that stores and transfers energy. In comparison, a resistor is an element that dissipates energy. If the stored energy lies in an electric field, the reactance is said to be *capacitive* in nature. Magnetic field storage elements are *inductors*. A capacitive reactance may then be defined as an element for which a relation can be written between charge, q and voltage, v, i.e.

$$q = f(v)$$

Similarly, an inductive element may be defined as one in which there is a relation between flux, ϕ and current, i, i.e.

$$\phi = f(i)$$

The essential feature of parametric amplifiers is that it utilizes a non-linear pure reactance, be it capacitive or inductive in nature. Since a pure reactance does not constitute to thermal noise in a circuit, parametric amplifiers should realise a low-noise amplification system.

Moreover, from (1.2), we see that thermal noise is a function of temperature. Lowering the temperature cannot eliminate shot noise in semiconductor junctions. Combining both of these conditions imply that there is a lower limit to which we can reduce noise in transistor circuitry and their operating at high temperatures increases noise levels. Therefore, realising parametric amplification is attractive for systems operating at extreme temperatures.

1.3. Parametric Amplification

Parametric amplification as demonstrated here in this project is based on capacitive devices. However, it can easily be extended to other forms of devices. The only requirement is that the quantity to be measured is partly dependent on a certain 'parameter', thus the name *parametric*. Take, for example, the amount of magnetic flux from an inductor coil.

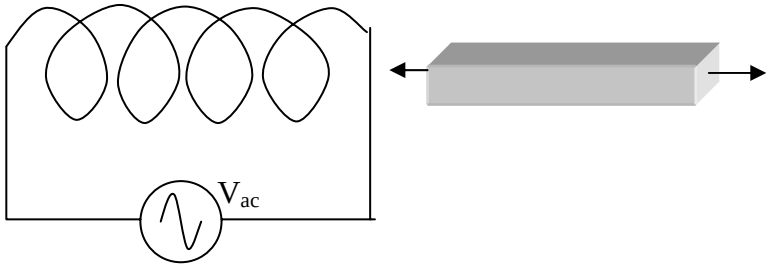

Fig. 1.2. A coil with a ferro-magnetic bar moving within it

As a varying potential of a frequency w_{ac} is applied across the coil, magnetic flux is induced in the coil. Suppose then that there is a ferro-magnetic bar moving in and out of the coil at a frequency of w_b. When the bar is within the coil, the effective permeability within the coil changes and a stronger magnetic flux is induced. In this case, the parameter which varies with time is the effective permeability within the coil, influenced by the motion of the bar. Fig. 1.2 shows the schematic of such a situation.

Now consider the situation if the bar is also moving at a frequency $w_b = 2w_{ac}$, and the amplitude coincides with the point where the bar is within the coil. If the phase between them is such that the maximum amplitude of the bar is at the time when the V_{ac} change is greatest, the amount of flux is effectively increased due to the presence of the bar within the coil. To the 'input' (V_{ac}), there appears to be gain because though it had been supplying constant power into the coil throughout, the magnetic flux generated is now apparently increased. This then is an example of a phase dependent parametric system since the increase in flux depends on whether the phase of the bar coincides with that of the applied voltage.

Various other forms of parametric amplification have been demonstrated before. Among them, the amplification of a weak spin wave (SW) in ferrite films [8], quantum dynamics [9], semiconductor junctions [10], microcantilevers [11] and MEMS devices [12].

Even among MEMS-based parametric amplification systems, the diversity in application is noted. Torsional oscillators [13], cantilevers [14], membranes [12] and a coupled resonator [15] have all been targets for parametric amplification.

One aspect of parametric amplification lies in the fact that various signals going in and out of the system must be free from one another's interference. The interaction between them must occur only within the device itself. As such, working in a single energy domain will require the use of some sort of filtering capability to ensure that the signals are decoupled within their own loops. An alternative would be to work in different energy domains. Thus various means of detection and actuation have been attempted, from piezo actuation [14] and detection [11] to light actuation [16] and detection [13].

1.4. Objectives

MEMS-based parametric amplifiers will greatly minimize the factors which hampered the progress of previous attempts. In this report, we will explore the possibility and constraints which make such MEMS-based parametric amplifiers an alternative for low noise systems. The aim is to demonstrate the existence of parametric amplification for low capacitance devices, of the order of a few pico-farads. The closest work to this is that of Raskin et al [12] where they used a 1 cm^2 size diaphragm as a parallel plate capacitor.

The initial phase of the project will be to understand and obtain a theoretical background for the operation of parametric amplification. To do this, the theory is adapted from one done by Blackwell [20] in which the operation using semiconductor diodes was derived. Acquiring the theory will allows us to have a better perceptive in selecting the best MEMS device available and spotting the potential pit-falls in the application. Ultimately, the goal is to demonstrate that low capacitance MEMS devices have the potential to be used as a parametric amplifier and verify that the operation agrees with theory.

In the process of characterizing the device, two new methodologies are discussed. Firstly, a novel method of measuring resonance through the measurement of signals at three times the driving frequency (termed *3f*) is demonstrated. Analysis of such detection scheme is done and verified with experimental results. The simplicity of the scheme allows it to be used for detecting resonance of one-port devices where parasitic capacitance is high, which other methods [17], [18] are incapable of.

A second methodology suggested is an Electrical Equivalent Modelling technique. By modelling mechanical parameters with electrical terms, it will be shown that it is possible to extract the mechanical values through the detection of electrical signals. However, this is limited to systems which are linear and where there is electrical-mechanical coupling. The usefulness of Bond Graphs is demonstrated by extending this capability to represent higher order systems.

1.5. Thesis Outline

The next chapter will introduce the analysis of excitation for capacitive-based MEMS devices. This is necessary to understand the issues faced in the detection of electrical signals as well as the *3f* method of detection.

In Chapter 3, the relations for parametric amplification systems are derived. Different configurations are analysed and the output relations are shown. Properties and theoretical characteristics of such a device are discussed as well.

Chapter 4 then shows the modelling of resonating circuits and the implications of parasitic capacitance. The electrical domain is shown to visualise such parasitics. A means

of using Bond Graphs to obtain equivalent higher degree-of-freedom systems is shown. Derivations of such electrical representations are shown to extract mechanical parameters.

Several device parameters are required to analyse the device fully and this is covered in Chapter 5. A novel *3f* detection scheme is introduced and discussed. A means of extracting the capacitance change ratio and internal resistance of the device is also introduced.

The last component necessary for the implementation of parametric amplifications is a filter. A basic outline of filters is covered in Chapter 6, and the resulting configuration that is used in this project is shown and analysed. A printed-circuit-board (PCB) design for the filters is presented.

Finally, Chapter 7 shows the final assembly of all the various issues discussed together with the results for a MEMS parallel-plate parametric amplifier. The experimental results for the various parameter extraction, resonance detection, filter design and parametric amplification are presented.

Chapter 8 concludes the project and proposes suggestions for future work.

CHAPTER 2: Capacitive-Based MEMS

The implementation of parametric amplification requires the existence of a time-varying capacitor. Capacitive-based MEMS devices suit this requirement perfectly. In this section, an introduction to such actuation means is presented.

2.1. MEMS device variation

Estimation of the actuation for capacitive-based devices has been established since Tang [19]. For any electrostatic capacitance, the energy stored, *E*, is known to be

$$E = \frac{1}{2} C V^2 \qquad 2.1$$

where C is the capacitance between the plates and V is the potential difference between them.

The actuation force is then

$$F = \frac{dE}{dx} = \frac{1}{2}\frac{dC}{dx} V^2 \qquad 2.2$$

Actuation force then depends on the nature of the capacitance variation with displacement, $\frac{dC}{dx}$. For a comb-drive, the capacitance change is approximately constant, within limits, as $C \approx \frac{2\varepsilon h(g_0 - x)}{d}$, where *h* is the depth of the finger for a single comb as shown in Fig. 2.1. Practical devices will contain many of such combs in parallel.

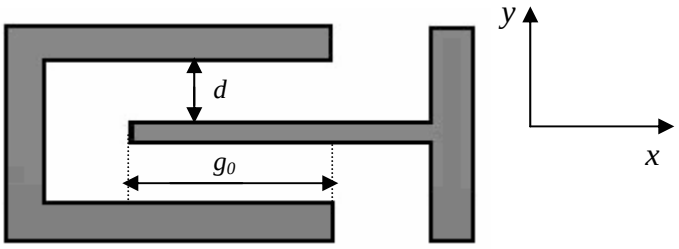

Fig. 2.1. Schematic for a single comb-drive

For a purely parallel plate, the capacitance change will approximately vary inversely with displacement since $C = \frac{\varepsilon A}{(d_0 - x)}$ (neglecting fringing fields), as shown in Fig. 2.2.

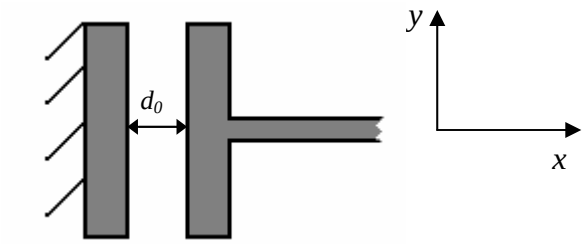

Fig. 2.2. Schematic for a movable parallel plate

2.2. Single and Double frequency actuation

Many capacitive-based devices like accelerometers and gyroscopes are necessarily resonated, mostly at their resonance frequencies. The actuation due to the applied voltages depends on the AC signal applied as well as the location of the placed voltages. For a 2-port device, an AC could be placed on one end, with a DC-bias on the mass and current detection at the other end (Fig. 2.3).

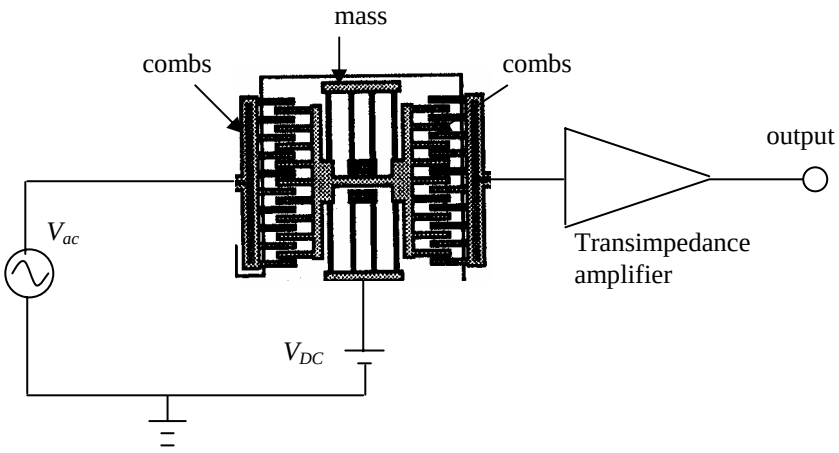

Fig. 2.3. Schematic of a resonator driven on one side

The V^2 term in (2.2) would be due to the difference in voltage of the AC and the DC applied i.e.

$$V = V_{ac} \sin wt - V_{dc}$$

Expanding the resulting force equation (2.2), the actuation force would then have components at frequencies of *w* and *2w*, as shown below

$$F = \frac{1}{2}\frac{dC}{dx}\left(V_{dc}^2 + \frac{V_{ac}^2}{2} - 2V_{dc}V_{ac}\sin wt - \frac{1}{2}V_{ac}^2 \cos 2wt\right) \qquad 2.3$$

The equilibrium position (which affects the mean capacitance, C_0) is also affected by the DC and AC voltages. Actuation is then at *w* as well as *2w*. The capacitance variation, which is dependent on the motion of the device, will also be at these two frequencies, i.e.

$$F(w,2w) \Rightarrow x(w,2w) \Rightarrow C(w,2w)$$

However, not all configurations will result in actuation and capacitance change at these frequencies. In another example, a 2-port device can be actuated *only* at *2w* if only an AC signal is applied to one side of the plate and the other side is grounded (Fig. 2.4).

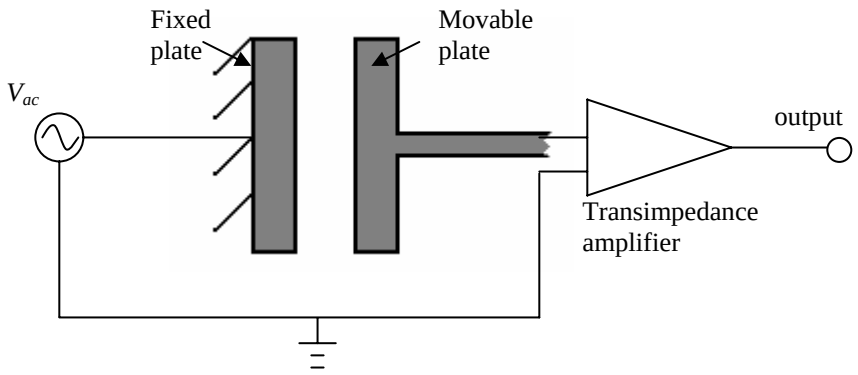

Fig. 2.4. Schematic for a single frequency actuation

In this case, $V = V_{ac} \sin wt$ and therefore,

$$F = \frac{1}{2}\frac{dC}{dx}\left(\frac{V_{ac}^2}{2} - \frac{V_{ac}^2}{2}\cos 2wt\right) \qquad 2.4$$

which shows an actuating signal at *2w*. In this scenario, the same AC signal affects the C_0 as well as resonates the structure. As will be shown in the results later, such approximations are not totally accurate. Due to the $\frac{dC}{dx}$ term being a function of *x* for a parallel plate configuration, excitation still occurs at *w*, albeit at much lower amplitudes.

Nevertheless, the desired operation or signal can be flexible and dependent on the requirement of the design and function of the device. We will see the application of such actuation in the next few chapters.

CHAPTER 3: Parametric Amplifier Theory

Manley and Rowe laid the foundations for parametric amplification in their 1956 paper. It is a paper that describes the theoretical limit and performance of parametric amplifiers. We begin by introducing the all-important Manley and Rowe's equations. Subsequently, we will see how the operating characteristics of MEMS devices fit into the picture and develop a theoretical model for four configurations: Up-converter Parametric Amplifier, Negative-Resistance Parametric Amplifier, Degenerate Amplifier and Phase-Coherent Degenerate Amplifier.

3.1. Manley-Rowe equations

Since the proposal of such an amplification system by Manley and Rowe in 1956, it has not been widely integrated due to various reasons, among them size, performance and application restrictions. However, the possibility of low-noise, high amplification is difficult to ignore. This is especially true in areas of space communications and systems operating at high temperatures, high sensitivity and low signal to noise (SNR) ratios.

The equations Manley & Rowe derived were based on a very simple circuit model as shown in Fig. 3.1.

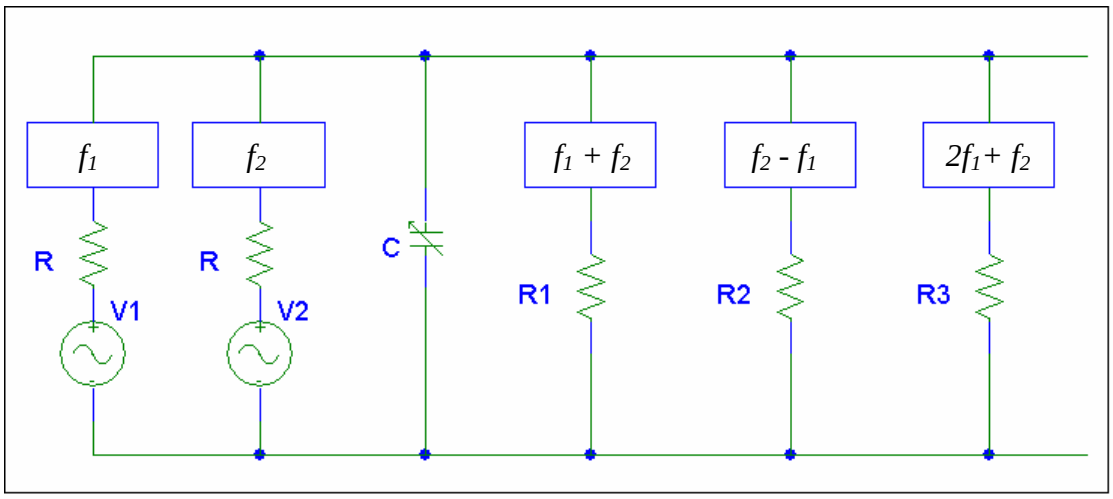

Fig. 3.1. Model which Manley-Rowe equations were based on

Essentially, the model comprised a non-linear capacitor (denoted by C in the figure) and two input sources, V1 and V2 operating at their own frequencies. f_1, f_2 and the

rest of the variations denotes some form of filters which restrict the *power* within each node to exist at only that particular frequency. R's denotes resistor for each node. The number of such output nodes goes effectively to infinity to encompass all possible permutations of frequencies f_1 and f_2.

The complete derivation can be found in [20]. The final result can be summed up by the following two equations:

$$\sum_{n=0}\sum_{m=-\infty}\frac{nP_{n,m}}{nf_s+mf_p}=0 \qquad 3.1$$

$$\sum_{n=-\infty}\sum_{m=0}\frac{mP_{n,m}}{nf_s+mf_p}=0 \qquad 3.2$$

where positive $P_{n,m}$ denotes power flowing *into* the non-linear capacitance and f_s and f_p represent the signal and pump frequencies respectively, applied to the device. The choice of which input is pump or signal is purely arbitrary. Expanding the equations for any n and m values expresses power levels at the various combinations of signal and pump frequencies.

Manley and Rowe's results were remarkable for two reasons: they are valid without specifying the exact characteristics of the non-linear capacitance as well as the power levels involved.

From these two fundamental relations, i.e. equations (3.1) and (3.2), the application of the theory then depends purely on the creativity of the designer. Though four frequency configurations are possible, we will only look at three frequency devices here [20]. The implications and characteristics of such parametric amplifiers will be derived below.

3.2. 3-frequency systems

We first look at the general operational characteristics obtainable from Manley-Rowe's equations.

For a 3-frequency system, other than a signal frequency f_1 and a pump frequency of f_2, the third frequency can be at the sum or difference of f_1 and f_2. Characteristics of both summing and difference systems are discussed in this section. Summing converters will be introduced first.

3.2.1. Summing converters

With only a third output frequency f_3 (which is the sum of f_1 and f_2), the resulting Manley-Rowe's equations become:

$$\frac{P_1}{f_1} + \frac{P_3}{f_3} = 0 \qquad 3.3$$

$$\frac{P_2}{f_2} + \frac{P_3}{f_3} = 0 \qquad 3.4$$

Even for summing converters, there are two summing situations that can be implemented: where $f_2 > f_1$ and $f_2 < f_1$.

To see the implications of the configurations, we represent the power signals on a power versus frequency plot, with arbitrary scales for the axes. As mentioned earlier, power going *into* the non-linear capacitance is given as positive and power out of it is negative. In this case, since we are supplying power at both the pump and signal frequencies, equations (3.3) and (3.4) tell us that the power output at frequency f_3 has to be negative. The arrows in bold in Fig.3.2. are the input and output signals which we should focus on, since the pump signal (f_2) is not the signal we are concerned with during amplification.

Fig. 3.2. shows the case of $f_2 > f_1$,

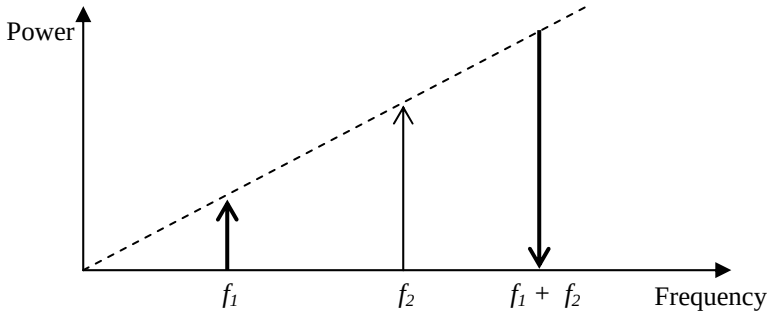

Fig. 3.2. Summing converters: $f_2 > f_1$

Fig. 3.3 shows the other case of $f_2 < f_1$,

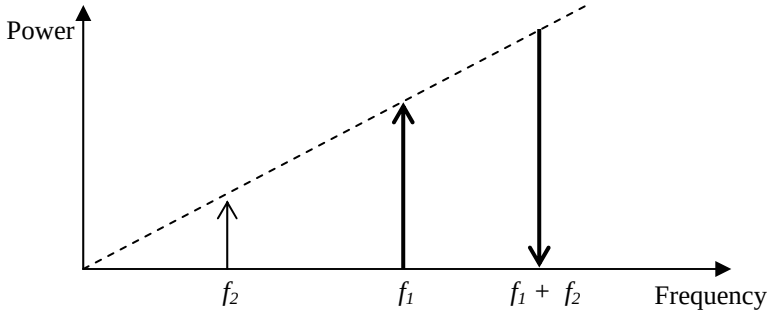

Fig. 3.3. Summing converter: $f_2 < f_1$

For both cases, the effective impedance of the device seen by both the signal and pump circuits is positive because power is dissipated at both frequencies and is therefore stable. The power gain we are interested in is the power of the output signal over the input signal, i.e. $\frac{P_3}{P_1}$ which can be shown to have the simple relation below

$$gain = \frac{f_3}{f_1} \qquad 3.5$$

which is just the ratio of the output and input frequencies. Such a configuration is termed an *up-converter*. This is the simplest implementation of a parametric configuration and its gain is always greater than unity, since f_3 is always greater than f_1. Optimally, we would want to operate at the configuration where $f_2 > f_1$ since a larger gain would be apparent. It must be noted that the Manley-Rowe equations express the theoretical maximum possible gain for such an operation. As will be shown later, the actual gain will always be less than this.

3.2.2. Difference converters

In a similar fashion, we can operate at difference frequencies of $f_4 = f_2 - f_1$ or $f_4 = f_1 - f_2$. For such configurations, the Manley-Rowe equations reduce to the form

$$\frac{P_1}{f_1} - \frac{P_4}{f_4} = 0 \qquad 3.6$$

$$\frac{P_2}{f_2} + \frac{P_4}{f_4} = 0 \qquad 3.7$$

If power is supplied at the pump, f_2, we see that power is delivered from the pump to both the output f_4 as well as the signal f_1. What this means is that the device delivers power to the signal rather than absorbing it. Again, there are two possible ways of implementation: $f_2 < f_1$ or $f_2 > f_1$.

Where in the case of $f_2 < f_1$, the power plot is shown in Fig. 3.4.

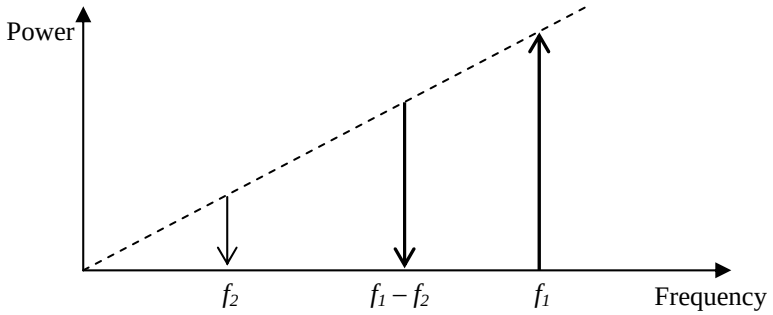

Fig. 3.4. Difference converters: $f_2 < f_1$

The input power at f_1 is higher than the output power f_4 and the difference is fed into the pump. Therefore, the effective impedance seen from the pump circuit is a negative resistance device. However, because the device itself would always possess a loss resistance, there is a possibility that the circuit might still remain stable if the signal is small enough or the internal resistance of the device is large enough. In addition, the gain would always be less than unity since $\frac{f_1 - f_2}{f_1} < 1$, as evident from the plot.

For the case of $f_2 > f_1$, the power plot is shown in Fig. 3.5.

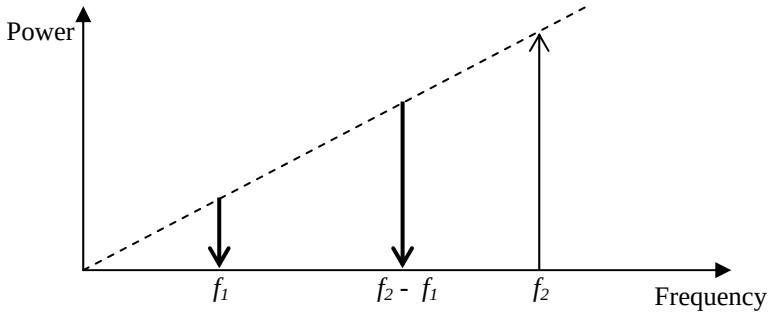

Fig. 3.5. Difference converters: $f_2 > f_1$

In this case, power is received by the signal as well as the output. The system is also then potentially unstable. It will be shown in the case of a Phase-Coherent

Degenerate Amplifier that the gain can be made as great as possible, whatever the ratio of the input and output frequencies.

What must be noted here is that there is no actual generation of power. Looking at the overall picture, there is simply a mixing of power after going through the non-linear device. Power is taken from certain output frequencies and transferred to others i.e. there is no change in the net power in the system. When the 'correct' frequencies are chosen, there appears to be amplification in the signal involved.

In the next few sections, detailed analysis and theoretical derivation of the various characteristics of parametric amplifiers are presented.

3.3. Small-Signal Analysis

We begin with the derivation for a general case. In this section, we approximate the case whereby the signal input is much lower than the pump signal; thus the analysis uses small signal approximations. The direction of the derivations is from Blackwell [20].

We attempt to derive a general formulation for gain of a parametric amplifier. As noted in the previous chapter, for a MEMS capacitive device, an approximation of the capacitance variance can consist mainly of two frequencies (neglecting all other harmonics)

$$C(t) = C_0\left(1 + 2\gamma_1 \cos w_2 t + 2\gamma_2 \cos 2w_2 t\right) \qquad 3.8$$

The coefficients γ_n represent the variation in capacitance at each frequency. The factor of 2 is included to simplify derivations later.

To derive a general formulation for the device, let the possible operating potentials be expressed as

$$v(t) = 2V_1 \cos w_1 t + 2V_2 \cos w_2 t + 2V_3 \cos w_3 t \qquad 3.9$$

The numbers of the subscripts represent the usual signals at the various potentials.
We know that current at output will be given by

$$i(t) = \frac{d}{dt}\left[C(t)v(t)\right] = C(t)\frac{dv(t)}{dt} + v(t)\frac{dC(t)}{dt} \qquad 3.10$$

Using small signal analysis, we write in phasor form,

$$C(t) = C_0 + C_0\gamma_1\left[e^{jw_2t} + e^{-jw_2t}\right] + C_0\gamma_2\left[e^{j2w_2t} + e^{-j2w_2t}\right]$$

$$v(t) = V_1e^{jw_1t} + V_1^*e^{-jw_1t} + V_4e^{jw_4t} + V_4^*e^{-jw_4t} + V_3e^{jw_3t} + V_3^*e^{-jw_3t}$$

$$i(t) = I_1e^{jw_1t} + I_1^*e^{-jw_1t} + I_4e^{jw_4t} + I_4^*e^{-jw_4t} + I_3e^{jw_3t} + I_3^*e^{-jw_3t}$$

Noting that $w_1 + w_2 = w_3$ and $w_2 - w_1 = w_4$, we are only interested in the real components of I_1 and I_3 and the imaginary component of I_4, i.e.

$$i(t) = I_1e^{jw_1t} + I_4^*e^{-jw_4t} + I_3e^{jw_3t}$$

Noting that

$$w_1 + w_2 = w_3$$

$$w_2 - w_1 = w_4$$

$$2w_2 = w_3 + w_4$$

the resulting relevant current components are

$$I_1 = jC_0V_1w_1 + jC_0\gamma_1V_3w_1 + jC_0\gamma_1V_4^*w_1$$

$$I_3 = jC_0\gamma_1V_1w_3 + jC_0V_3w_3 + jC_0\gamma_2V_4^*w_3$$

$$I_4^* = -jC_0\gamma_1V_1w_4 - jC_0\gamma_2V_3w_4 - jC_0V_4^*w_4$$

The admittance matrix of the device can then be written as

$$\begin{bmatrix} I_1 \\ I_3 \\ I_4^* \end{bmatrix} = \begin{bmatrix} jC_0w_1 & jC_0\gamma_1w_1 & jC_0\gamma_1w_1 \\ jC_0\gamma_1w_3 & jC_0w_3 & jC_0\gamma_2w_3 \\ -jC_0\gamma_1w_4 & -jC_0\gamma_2w_4 & -jC_0w_4 \end{bmatrix} \begin{bmatrix} V_1 \\ V_3 \\ V_4^* \end{bmatrix} \qquad 3.11$$

This general formulation will be utilized for the Up-Converter and the Negative-Resistance configurations.

3.4. Up-Converter Parametric Amplifier

For an up-converter, the output frequency is at the sum of f_1 and f_2. The circuit for such a configuration is shown in Fig. 3.6.

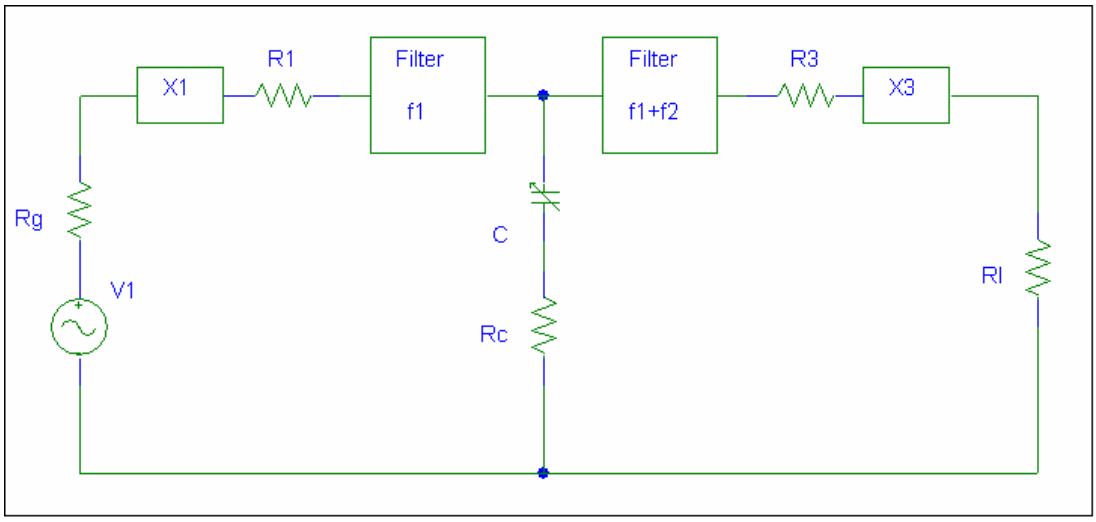

Fig. 3.6. Schematic of up-converter circuitry

The time-varying capacitor is pumped at a certain frequency f_2, not noted in the schematic. R_g represents the internal resistance of the input signal. X_1 and R_1 represent the reactance and resistance of the input circuit respectively and R_c represents the internal loss of the device. R_l is the load.

For an up-converter working on only two frequencies, the matrix (3.11) reduces to

$$\begin{bmatrix} I_1 \\ I_3 \end{bmatrix} = \begin{bmatrix} jC_0 w_1 & jC_0 \gamma_1 w_1 \\ jC_0 \gamma_1 w_3 & jC_0 w_3 \end{bmatrix} \begin{bmatrix} V_1 \\ V_3 \end{bmatrix} \qquad 3.12$$

in which the relevant frequencies concerned are at the input frequency f_1 and the summed frequency f_3.

By inversing, the impedance matrix is then

$$\begin{bmatrix} V_1 \\ V_3 \end{bmatrix} = \begin{bmatrix} \dfrac{1}{jw_1 C_0 (1-\gamma_1^2)} & \dfrac{-\gamma_1}{jw_3 C_0 (1-\gamma_1^2)} \\ \dfrac{-\gamma_1}{jw_1 C_0 (1-\gamma_1^2)} & \dfrac{1}{jw_3 C_0^2 (1-\gamma_1^2)} \end{bmatrix} \begin{bmatrix} I_1 \\ I_3 \end{bmatrix} = \begin{bmatrix} Z_{11} & Z_{12} \\ Z_{21} & Z_{22} \end{bmatrix} \begin{bmatrix} I_1 \\ I_3 \end{bmatrix} \qquad 3.13$$

where subscripts 1 and 3 denote the voltages and currents at input and output frequencies respectively. The impedance relation models a four terminal network. Such a system can be depicted as in Fig. 3.7.

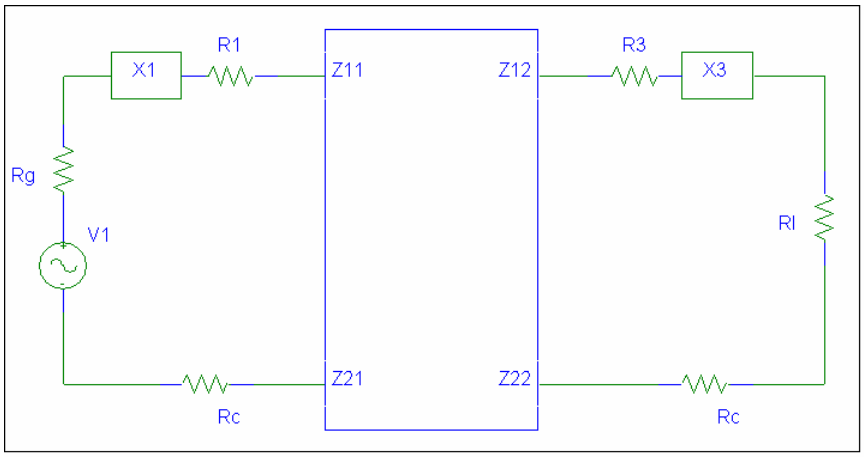

Fig. 3.7. A four terminal network model

Now, if we were to include all the various impedances into our 4-port model, (3.13) will have the form

$$\begin{bmatrix} V_1 \\ V_3 \end{bmatrix} = \begin{bmatrix} Z_{11} + Z_{T1} & Z_{12} \\ Z_{21} & Z_{22} + Z_{T3} \end{bmatrix} \begin{bmatrix} I_1 \\ I_3 \end{bmatrix} \qquad 3.14$$

where

$$Z_{T1} = R_g + X_1 + R_1 + R_c \qquad 3.15$$

$$Z_{T3} = R_l + X_3 + R_3 + R_c \qquad 3.16$$

Now, we attempt to find the power gain at the load of the system. The maximum power input possible (from the maximum power theorem) is $\left|\frac{V_1}{2}\right|^2 \frac{1}{R_g} = \frac{|V_1|^2}{4R_g}$. The power output at the load is $|I_3|^2 R_l$.

The power gain is then, $g_t = \dfrac{4R_g R_l |I_3|^2}{|V_1|^2}$

It is necessary then to express a relation that relates the current output I_3 in terms of input voltage V_1. From (3.14), and letting $V_3 = 0$ (as there is no actual source voltage at output), we can show that

$$I_3 = -\frac{Z_{21} V_1}{(Z_{22} + Z_{T3})(Z_{11} + Z_{T1}) - Z_{21} Z_{12}} \qquad 3.17$$

The gain is then of the form

$$g_t = \frac{4R_l R_g \left|Z_{21}\right|^2}{\left|\left(Z_{22}+Z_{T3}\right)\left(Z_{11}+Z_{T1}\right)-Z_{21}Z_{12}\right|^2} \qquad 3.18$$

For the circuit to be operating at resonance, there should not be any reactance, i.e. $Z_{11}+X_1=0$ and $Z_{22}+X_3=0$. Also substituting the other impedances into the equation, we obtain the approximate value of g_t as

$$g_t = \frac{4R_l R_g \left|\frac{\gamma_1}{w_1 C}\right|^2}{\left|\left(R_l+R_c+R_3\right)\left(R_g+R_c+R_1\right)+\frac{\gamma_1^2}{w_1 w_3 C^2}\right|^2} \qquad 3.19$$

where

$$C = C_0\left(1-\gamma_1^2\right) \qquad 3.20$$

We can, if appropriate for the device in question, make another assumption that the circuit losses are negligible compared to the device losses, i.e. $R_3 << R_l + R_c$ and $R_1 << R_g + R_c$. The gain equation would then look like the following, after simplification

$$g_t = \frac{4R_l R_g}{\left[\left(R_l+R_c\right)\left(R_g+R_c\right)\frac{w_1 C}{\gamma_1}+\frac{\gamma_1}{w_3 C}\right]^2} \qquad 3.21$$

To find the maximum gain g_t, we are interested to know what load and internal resistance values would maximize gain. This is a characteristic which differentiates parametric amplification from 'normal' circuits. The load that achieves maximum power transfer is not fixed with respect to the internal load of the source, but can be changed by varying another parameter, γ_1. We can obtain optimal expressions for R_l and R_g from (3.21) separately.

$$R_l = \frac{\left(R_g R_c + R_c^2\right)\frac{w_1 C}{\gamma_1}+\frac{\gamma_1}{w_3 C}}{\left(R_g+R_c\right)\frac{w_1 C}{\gamma_1}} \qquad 3.22$$

The expression for R_g is similar (simply substituting terms containing R_g with R_l). In this case, the gain is optimized for a given source impedance R_g and γ_1. The corresponding R_l is then obtained for this set of values.

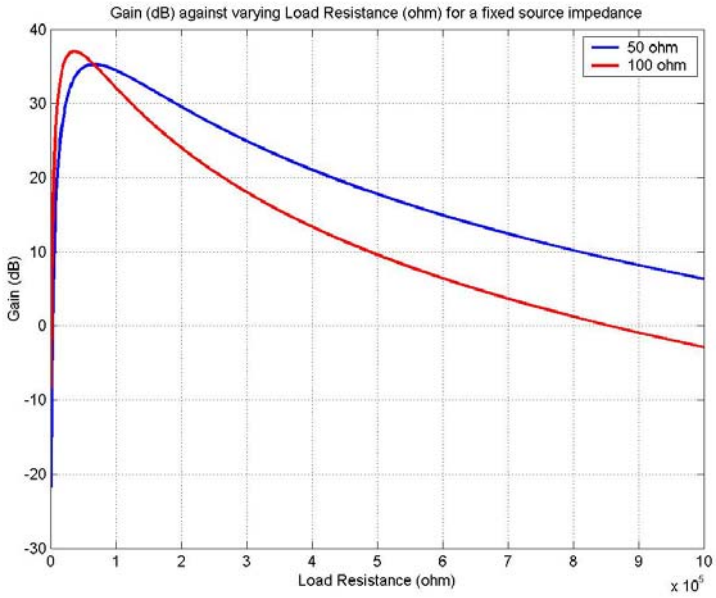

Fig. 3.8. Plot showing the theoretical relation between gain and load.

Fig. 3.8 shows the relation between gain and load resistance R_l when the source impedance is fixed at values of 50 Ω and 100 Ω and $\gamma_1 = 0.002$. In essence, there is an optimal R_l that achieves maximum gain for different values of source impedance.

Alternatively, we can also obtain an expression where both optimal resistance values 'meet'. This would also imply that whatever expression which maximizes for R_l would do the same for R_g. Then $R_g = R_l$ for maximum gain. Differentiating g_t with respect to R_g in equation (3.21) to find the optimal R_g gives

$$R_g = R_c \sqrt{1 + \frac{\gamma_1^2}{w_1 w_3 C^2 R_c^2}} \qquad 3.23$$

This expression then dictates the values of R_g and R_l which will optimize the gain for a given γ.

To show that the gain is truly bounded by Manley-Rowe's equations, defining $Q = \frac{1}{w_1 C R_c}$ as the effective *Q* of the capacitive device at w_1, we have

$$R_g = R_c \sqrt{1 + \frac{w_1}{w_3}(\gamma_1 Q)^2} \qquad 3.24$$

We then substitute this expression back into (3.21),

$$g_t = \frac{w_3}{w_1} \frac{x}{\left[1 + \sqrt{1+x}\right]^2} \qquad 3.25$$

where $x = \left(\frac{w_1}{w_3}\right)(\gamma_1 Q)^2$.

The term $\frac{x}{\left[1 + \sqrt{1+x}\right]^2} \to 1$ as $x \to \infty$, by applying L'Hopital's rule.

Since the value of γ_1 is bounded (from 0 to 0.5, from the definition), to obtain an infinite value of *x*, we would require $Q \to \infty$, which implies a lossless device.

Thus it is shown that a parametric amplification system is limited by Manley-Rowe equations. In practice, to get the maximum gain possible from the system, we would require the parameter γ_1 be as large as possible, which implies that the device is operating at resonance. Therefore, the pump frequency f_2 will give optimal performance if operated at the resonant frequency of the structure.

3.4.1 Input and Output Impedances

It was shown previously that a standard 4-terminal network model could approximate the device characteristics. The effective input impedance can be obtained through the standard form of

$$Z_{in} = Z_{11} - \frac{Z_{12} Z_{21}}{Z_{22} + Z_{T4}} \qquad 3.26$$

Substituting the relevance parameters from (3.13) into (3.26) we have,

$$Z_{in} = \frac{1}{jw_1 C} + \frac{\gamma^2}{w_1 w_3 C^2 \left(Z_{T3} + \frac{1}{jw_3 C}\right)} \qquad 3.27$$

At circuit resonance, we are left with only the real values, which will be

$$R_{in} = \frac{\gamma^2}{w_1 w_3 C^2 R_{T3}} \tag{3.28}$$

which is a positive value.

By symmetry, the effective output impedance the capacitor presents to the output circuit at resonance is then

$$R_{out} = \frac{\gamma^2}{w_1 w_3 C^2 R_{T1}} \tag{3.29}$$

Since both effective input and output resistance values are positive, the operation of the up-converter device is stable.

3.5. Negative-Resistance Parametric Amplifier

For this mode of operation, the output frequency is at the difference frequencies of pump and signal. As the name suggests, the effective impedance of the device will be shown to be negative. For such a case, the matrix is given as

$$\begin{bmatrix} I_1 \\ I_4^* \end{bmatrix} = \begin{bmatrix} jC_0 w_1 & jC_0 \gamma_1 w_1 \\ -jC_0 \gamma_1 w_4 & -jC_0 w_4 \end{bmatrix} \begin{bmatrix} V_1 \\ V_4^* \end{bmatrix} \tag{3.30}$$

and the impedance matrix as

$$\begin{bmatrix} V_1 \\ V_4^* \end{bmatrix} = \begin{bmatrix} \frac{1}{jw_1 C_0 (1-\gamma_1^2)} & \frac{\gamma_1}{jw_4 C_0 (1-\gamma_1^2)} \\ \frac{-\gamma_1}{jw_1 C_0 (1-\gamma_1^2)} & \frac{-1}{jw_4 C_0^2 (1-\gamma_1^2)} \end{bmatrix} \begin{bmatrix} I_1 \\ I_4^* \end{bmatrix} = \begin{bmatrix} Z_{11} & Z_{12} \\ Z_{21} & Z_{22} \end{bmatrix} \begin{bmatrix} I_1 \\ I_4^* \end{bmatrix} \tag{3.31}$$

As in the case of the up-converter, the matrix equation has to include the various impedances in the circuit. In this case, the circuit model is depicted in Fig. 3.9.

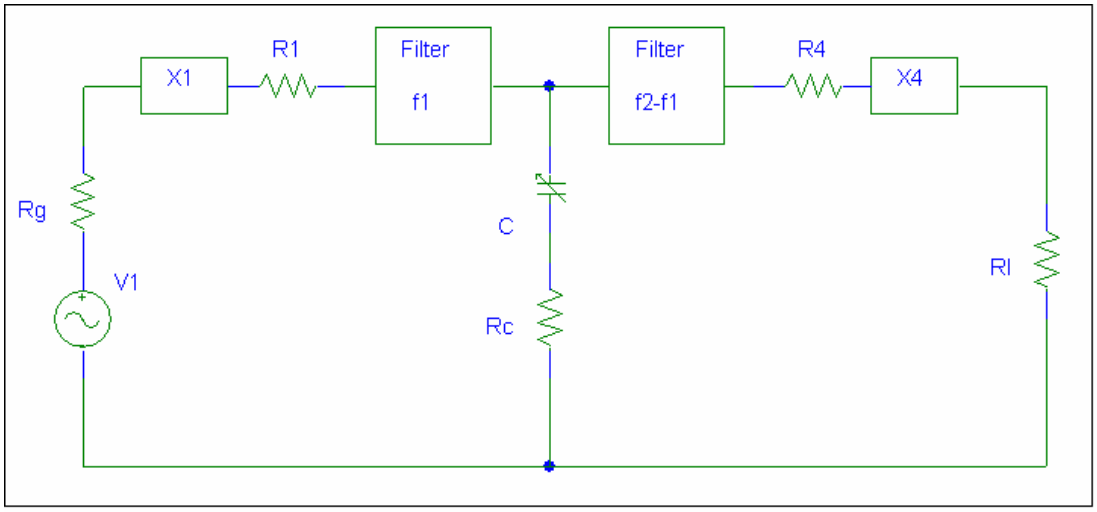

Fig. 3.9. Circuit model for a negative resistance amplifier

Thus,

$$\begin{bmatrix} V_1 \\ V_4^* \end{bmatrix} = \begin{bmatrix} Z_{11} + Z_{T1} & Z_{12} \\ Z_{21} & Z_{22} + Z_{T4} \end{bmatrix} \begin{bmatrix} I_1 \\ I_4^* \end{bmatrix} \tag{3.32}$$

where

$$Z_{T1} = R_g + X_1 + R_1 + R_c$$

$$Z_{T4} = R_l + X_4 + R_4 + R_c$$

With $V_4^* = 0$, we write I_1 as a function of V_1,

$$I_1 = \frac{-V_1 Z_{21}}{(Z_{11} + Z_{T1})(Z_{22} + Z_{T4}) - Z_{12} Z_{21}} \tag{3.33}$$

The power gain is given by

$$g_t = \frac{4R_g R_l |I_2|^2}{|V_1|}$$

$$= \frac{4R_g R_l |Z_{21}|^2}{\left|(Z_{11} + Z_{T1})(Z_{22} + Z_{T4}) - Z_{12} Z_{21}\right|^2} \tag{3.34}$$

At resonance then,

$$g_t = \frac{w_4}{w_1} \frac{4R_g R_l \left(\frac{R}{R_{T4}}\right)}{[R_{T1} - R]^2} \tag{3.35}$$

where $R = \dfrac{\gamma^2}{w_1 w_4 C^2 R_{T4}}$.

This configuration is not particularly interesting beyond the fact that the input source 'sees' a negative impedance. As such the system is possibly oscillatory and unstable.

3.6. Degenerate Amplifier

We now look at a different possible configuration of parametric amplifiers: a degenerate amplifier. The configuration operates at the difference frequency of $f_4 = f_2 - f_1$. There are again two subsets which can occur. Firstly, the relation between pump and signal is such that the output frequency f_4 lies within the passband of the signal or vice versa. Another, termed a phase-coherent amplifier, lies in the fact that the desired operating output frequency f_4 is also the input frequency at f_1. Therefore, filters will not be able to tell the difference between the two signals. Some interesting characteristics result.

To analyse the configuration, we look at the circuit model which will be used to derive the operating characteristics.

We will go on to show that the gain characteristic is dependent on the phase difference of the pump and signal. As such, we will use trigonometric representations with phase information to derive the gain relations.

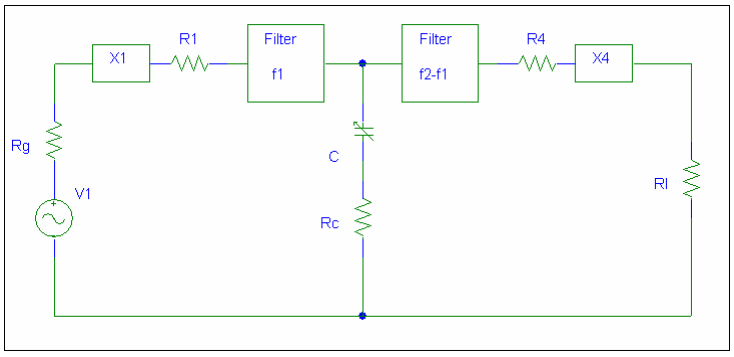

Fig. 3.10. Original voltage model

In this case, instead of using the usual voltage model in Fig. 3.10, we look at a current equivalent circuit model as shown in Fig. 3.11. This is done so as to express the phase-relations for the current output explicitly.

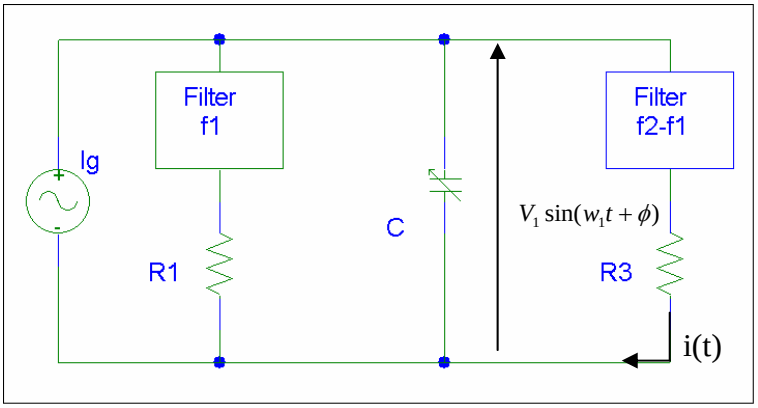

Fig. 3.11. Equivalent current source model

As before, we are interested in the power gain. In a similar fashion, the maximum power that can be supplied by the source, this time an equivalent current source is $\left(\frac{i_g}{2}\right)^2 R_1$.

The power output at resistor R_4 is $\frac{V_1^2}{R_4}$. Therefore, the power gain is

$$g_t = \frac{4V_1^2}{|i_g|^2 R_1 R_4} \qquad 3.36$$

An expression that relates current to voltage will result in a full equation of the power gain of the configuration. We proceed to derive current in terms of voltage. From this point on, we will depart from the derivations of Blackwell [20]. There are several errors in his derivations, the main one being adding an unknown phase to the capacitance change expression.

As a convention, positive voltage will be represented as depicted in Fig. 3.11. Again, we know that

$$i(t) = \frac{d}{dt}\left[C(t)v(t)\right] = C(t)\frac{dv(t)}{dt} + v(t)\frac{dC(t)}{dt}$$

where positive current is 'downward' as shown in the Fig. 3.11.

Let the capacitance change be

$$C(t) = C_0\left(1 + 2\gamma_1 \sin w_2 t + 2\gamma_2 \sin 2w_2 t\right)$$

The filters allow the presence of frequencies at w_1 and w_4, i.e.

$$v(t) = V_1 \sin(w_1 t + \phi_1) + V_4 \sin(w_4 t + \phi_4)$$

where the unknown phase changes are included as some unknown phases ϕ_1 and ϕ_4.

Looking at $C\frac{dv}{dt}$ first, the various relevant components are

$$\begin{aligned} & C_0\left[V_1 w_1 \cos(w_1 t + \phi_1) + V_4 w_4 \cos(w_4 t + \phi_4)\right] \\ & + \gamma_1 C_0 V_1 w_1\left[\sin((w_2 + w_1)t + \phi_1) + \sin((w_2 - w_1)t - \phi_1)\right] \\ & + \gamma_1 C_0 V_3 w_3\left[\sin((w_4 + w_2)t + \phi_4) + \sin((w_2 - w_4)t - \phi_4)\right] \end{aligned} \qquad 3.37$$

Relevant components within $v\frac{dC}{dt}$ are

$$\begin{aligned} & + \gamma_1 C_0 V_1 w_2\left[\sin((w_1 + w_2)t + \phi_1) - \sin((w_2 - w_1)t - \phi_1)\right] \\ & + \gamma_1 C_0 V_4 w_2\left[\sin((w_4 + w_2)t + \phi_4) - \sin((w_2 - w_4)t - \phi_4)\right] \end{aligned} \qquad 3.38$$

For reasons which will be apparent later, the current through the device that is relevant to us is only those at $(w_2 - w_1)$ and $(w_2 - w_4)$ i.e.

$$\begin{aligned} & \gamma_1 C_0 V_1 w_1 \sin\left[(w_2 - w_1)t - \phi_1\right] + \gamma_1 C_0 V_4 w_4 \sin\left[(w_2 - w_4)t - \phi_4\right] \\ & - \gamma_1 C_0 V_1 w_2 \sin\left[(w_2 - w_1)t - \phi_1\right] - \gamma_1 C_0 V_4 w_2 \sin\left[(w_2 - w_4)t - \phi_4\right] \end{aligned} \qquad 3.39$$

which can be further simplified to give

$$i = -\gamma_1 C_0 V_1 w_4 \sin(w_4 t - \phi_1) - \gamma_1 C_0 V_4 w_1 \sin(w_1 t - \phi_4) \qquad 3.40$$

The negative sign means that instead of current flowing 'into' the device, it is actually supplying current to the system. This is visualized in Fig. 3.12.

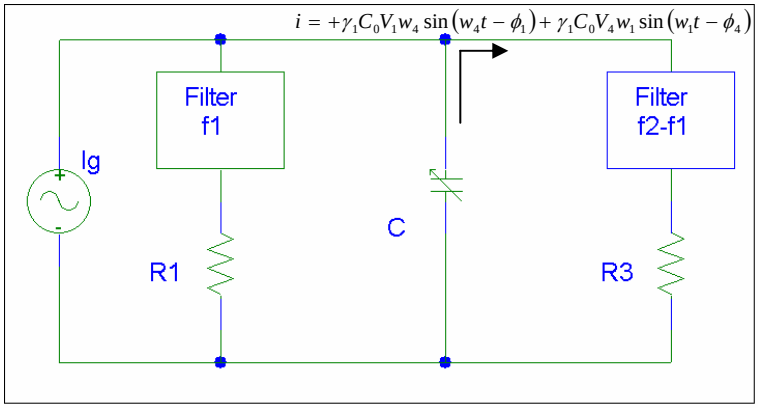

Fig. 3.12. Circuit model showing direction of current flow

Now, based on the assumed potential, the current flowing into the individual resistors are

$$i_{R_1} = \frac{V_1}{R_1}\sin(w_1 t + \phi_1) + \frac{V_4}{R_1}\sin(w_4 t + \phi_4)$$

and

$$i_{R_4} = \frac{V_1}{R_4}\sin(w_1 t + \phi_1) + \frac{V_4}{R_4}\sin(w_4 t + \phi_4)$$

The components at w_4 frequency are not from the input, thus it must have been 'sourced' from the varying capacitor. So we have

$$V_4\left(\frac{1}{R_1}+\frac{1}{R_4}\right)\sin(w_4 t + \phi_4) = \gamma_1 C_0 V_1 w_4 \sin(w_4 t - \phi_1) \qquad 3.41$$

From the above equation (3.41), we can obtain expressions relating (V_4, ϕ_4) to (V_1, ϕ_1)

$$\Rightarrow \begin{cases} V_4\left(\frac{1}{R_1}+\frac{1}{R_4}\right)\cos\phi_4 = \gamma_1 C_0 V_1 w_4 \cos\phi_1 \\ V_4\left(\frac{1}{R_1}+\frac{1}{R_4}\right)\sin\phi_4 = -\gamma_1 C_0 V_1 w_4 \sin\phi_1 \end{cases}$$

$$\Rightarrow \begin{cases} V_4\cos\phi_4 = \gamma_1 C_0 V_1 w_4 \cos\phi_1\left(\frac{R_1 R_4}{R_1+R_4}\right) \\ V_4\sin\phi_4 = -\gamma_1 C_0 V_1 w_4 \sin\phi_1\left(\frac{R_1 R_4}{R_1+R_4}\right) \end{cases} \qquad 3.42$$

Now we can look at the expression for the source current, which can only be sourcing at w_1

$$i_g(w_1) = \frac{V_1}{R_1}\sin(w_1 t + \phi_1) + \frac{V_1}{R_4}\sin(w_1 t + \phi_1) - \gamma_1 C_0 V_4 w_1 \sin(w_1 t - \phi_4)$$

$$= V_1\left(\frac{1}{R_1}+\frac{1}{R_4}\right)\sin(w_1 t + \phi_1) - \gamma_1 C_0 w_1 V_4 \sin(w_1 t - \phi_4) \qquad 3.43$$

The whole purpose of (3.42) is to substitute into (3.43) to express everything in terms of V_1.

We know that

$$V_4 \sin(w_1 t - \phi_4) = V_4 [\sin w_1 t \cos\phi_4 - \cos w_1 t \sin\phi_4]$$
$$= \gamma_1 C_0 V_1 w_4 \frac{R_1 R_4}{R_1 + R_4} [\sin w_1 t \cos\phi_1 + \cos w_1 t \sin\phi_1]$$
$$= \gamma_1 C_0 V_1 w_4 \frac{R_1 R_4}{R_1 + R_4} \sin(w_1 t + \phi_1)$$

Therefore, the final expression for the source current is

$$i_g(w_1) = V_1 \left(\frac{1}{R_1} + \frac{1}{R_4} \right) \sin(w_1 t + \phi_1) - \left(\frac{R_1 R_4}{R_1 + R_4} \right) (\gamma_1 C_0)^2 w_1 w_4 V_1 \sin(w_1 t + \phi_1) \qquad 3.44$$

The gain expression is then

$$g_t = \frac{4}{R_1 R_4 \left[\left(\frac{R_1 + R_4}{R_1 R_4} \right) - \left(\frac{R_1 R_4}{R_1 + R_4} \right) (\gamma_1 C_0)^2 w_1 w_4 \right]^2} \qquad 3.45$$

Thus we have derived the gain equation for a case where $w_1 \neq w_4$.

3.7. Phase-Coherent Degenerate Amplifier

A more interesting case is of a phase-coherent amplifier, $w_1 = w_4 = \frac{1}{2} w_2$.

In this manner, there is a presence of only

$$v(t) = V_1 \sin(w_1 t + \phi_1)$$

The mixing of the signal and capacitance produces a current at

$$i_c(w_1) = -w_1 \gamma_1 C_0 V_1 \sin(w_1 t - \phi_1)$$

The generator current is then

$$i_g = V_1 \left(\frac{1}{R_1} + \frac{1}{R_4} + w_1 C_0 \right) \sin(w_1 t + \phi_1) - \gamma_1 C_0 w_1 V_1 \sin(w_1 t - \phi_1)$$

In this case, the gain is dependent on the phase of the signal. To see that relation, we have to work in complex notation,

$$i_g = e^{i w_1 t} \left[V_1 \left(\frac{1}{R_1} + \frac{1}{R_4} + w_1 C_0 \right) e^{j\phi_1} - V_1 \gamma_1 C_0 w_1 e^{-j\phi_1} \right]$$

To get the magnitude of current, we take the conjugate,

$$\left|i_g\right|^2 = i_g i_g^* = \left[V_1\left(\frac{1}{R_1}+\frac{1}{R_4}+w_1C_0\right)\right]^2\left[1-\frac{2\gamma_1 C_0 w_1}{\left(\frac{1}{R_1}+\frac{1}{R_4}+w_1C_0\right)}e^{2j\phi_1}+\left(\frac{\gamma_1 C_0 w_1}{\left(\frac{1}{R_1}+\frac{1}{R_4}+w_1C_0\right)}\right)^2\right]$$

Now, if we let

$$\beta = \frac{\gamma_1 C_0 w_1}{\frac{1}{R_1}+\frac{1}{R_4}+w_1C_0} \qquad 3.46$$

the expression can be rewritten as

$$g_t = \frac{4}{\left(\frac{1}{R_1}+\frac{1}{R_4}+w_1C_0\right)^2 R_1R_4\left[1+\beta^2-2\beta\sin(2\phi)\right]} \qquad 3.47$$

which shows gain being a function of the phase difference between the signal and the pump frequency.

To determine the phase which will give us maximum gain, we want the denominator to be as small as possible, therefore

$$\sin(2\phi) = 1$$

$$\Rightarrow \phi = \frac{\pi}{4}$$

To maximise the gain at optimal phase, i.e.

$$g_t\left(\phi=\frac{\pi}{4}\right) = \frac{4}{\left(\frac{1}{R_1}+\frac{1}{R_4}+w_1C_0\right)^2 R_1R_4\left[1+\beta^2-2\beta\right]} = \frac{4}{\left(\frac{1}{R_1}+\frac{1}{R_4}+w_1C_0\right)^2 R_1R_4\left[\beta-1\right]^2}$$

β should be as close to 1 as possible. Parameters which we can vary easily are C_0, w_1 and γ_1. Figure 3.13 shows the phase-related gain.

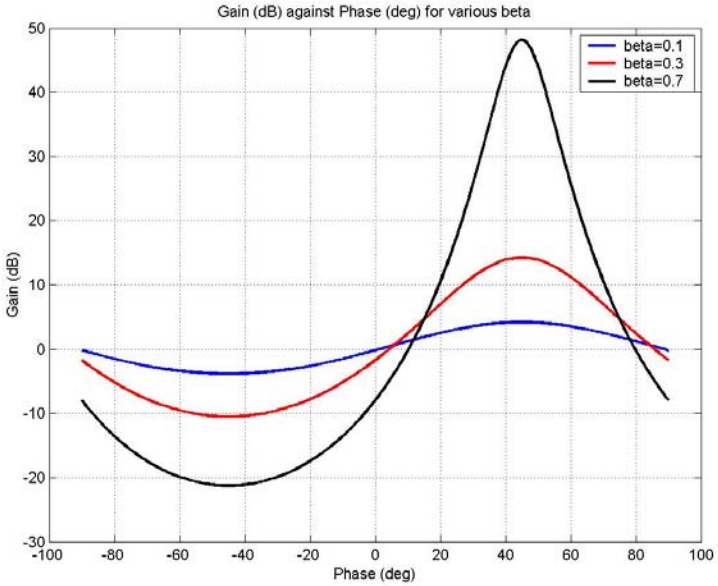

Fig. 3.13. Plot of phase related gain

This configuration demonstrates a highly phase-selective amplifier if certain parameters are met. Possible uses can be as for a phase-lock loop system.

CHAPTER 4: Modelling

4.1. Introduction

MEMS is a field which crosses multiple disciplines; from mechanical to electrical to materials science. In actuation and sensing of capacitive-based devices, there is coupling between the mechanical and electrical domains which has to be addressed. Modelling of such devices then would have to take into account such multi-energy effects. In this section, a means of incorporating mechanical aspects in the electrical domain will be presented. Its usefulness will be explored for simple linear systems.

The proposed approach makes use of Bond Graphs [21], a modelling technique first formulated by Professor Henry Paynter in the 1950s. Bond Graphs allows the ability to represent multi-energy domains in a single graphical form and also obtain state-space equations from them.

4.2. 1-DOF Equivalent Electrical Model

Bond graphs provide a means of representing multi-energy domains in a single pictorial format. The usefulness is therefore apparent in MEMS, where we are dealing with coupled systems. However, the final detection is always performed on electrical systems and that is where all the various cross-coupling within the system, is finally 'seen'. What will be presented here is a method of representing and analysing mechanical systems in the electrical domain.

The well-known mechanical vibration equation for a single degree-of-freedom (DOF), i.e.

$$m\ddot{x} + c\dot{x} + kx = F_0 \qquad 4.1$$

where the notations represent the usual forms, is a simple representation of a linear mechanical device. It is the basis of MEMS resonating structures. In Table 4.1 we compare and see the relations between Bond Graph elements, electrical elements and mechanical elements (see also Appendix A).

Table 4.1: Showing relations between Bond Graph, Mechanical and Electrical elements

Symbol	Bond Graph		Mechanical	Electrical
Effort	e		*Force, F*	*Potential, v*
Flow	f		*Velocity,* $\dot{x}$	*Current,* $i = \dot{Q}$
	General Relation	Linear Relation		
Resistor	$e = \phi_R(f)$	$e = Rf$	$F = c\dot{x}$	$v = iR = R\dot{Q}$
Capacitor	$q = \phi_C(e)$ $e = \phi_C^{-1}(q)$	$e = \frac{1}{C}q$	$F = kx$	$i = C\frac{dv}{dt}$ $\Rightarrow v = \frac{1}{C}\int i dt = \frac{1}{C}Q$
Inductor	$p = \phi_I(f)$ $f = \phi_I^{-1}(p)$	$p = If$ $f = \frac{p}{I}$	$F = m\ddot{x}$	$v = L\frac{di}{dt} = L\ddot{Q}$

What is seen is a one-to-one relation between elements in the two domains: capacitor equivalent to springs, resistors equivalent to dampers and inductors behaving similar to mass. Bond Graph modelling utilizes such multi-domain characteristics. Of course, these relations are not exhaustive. Fluid dynamics, thermodynamics, optics, etc all have their equivalent elements. Electrical and mechanical domains are shown here because these are the two main domains which MEMS devices operate in.

What is intended here is to demonstrate a means of representing simple mechanical systems entirely using electrical components. This approach is not new. Clark [22] had already used such electrical schematics to represent mechanical resonating devices. From an electrical background, his objective was to visualise mechanical systems in the electrical domain. However, this chapter will show that its capability can be extended beyond just visualisation.

We will begin by looking at single-DOF mechanical devices, where the equation of motion is the simple (4.1)

$$m\ddot{x} + c\dot{x} + kx = F_0$$

The equation says that the “summation of the forces due to inertia, damper and spring of the system must be equal to the external forces” acting on the system. From Table 4.1

above, we know that there should be an equivalent electrical model. To paraphrase the line above: "summation of the *potential* due to *inductor*, *resistor* and *capacitor* of the system must be equal to the external *potentials*" i.e.

$$inductor + resistor + capacitor = V$$

or in terms of conventional parameters,

$$L\frac{di}{dt} + Ri + \frac{1}{C}\int idt = V$$

Such a circuit then would be an inductor, capacitor and resistor (LCR) connected in series, as shown in Fig. 4.1 below

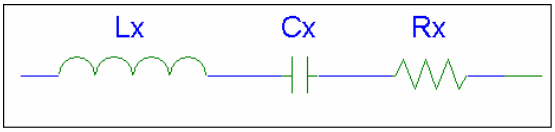

Fig. 4.1. Equivalent electrical model

Both electrical and mechanical models exhibit the characteristic of resonance, as expected. We will see below how this electrical model helps us better visualize the concept of parasitics.

4.3. Parasitic Capacitance

The presence of parasitic capacitance greatly complicates the detection and performance of capacitive-based devices. Parasitic exists between probe tips, wiring, static structures on the devices, etc. It is unavoidable but its effects can be minimized through proper design and consideration of possible causes. Depending on the situation, parasitics can range from a few picofarads to even hundreds of picofarads. Thus, for a device which has perhaps a few picofarads of capacitance change (depending on design), it is easily seen why it can pose problems.

With the equivalent electrical model obtained above (Fig. 4.1), incorporating parasitics into the model is simply a matter of adding a capacitor in parallel with the circuit, i.e. parasitic capacitance is a capacitance value that exists 'on top of' the actual device as represented in Fig. 4.2.

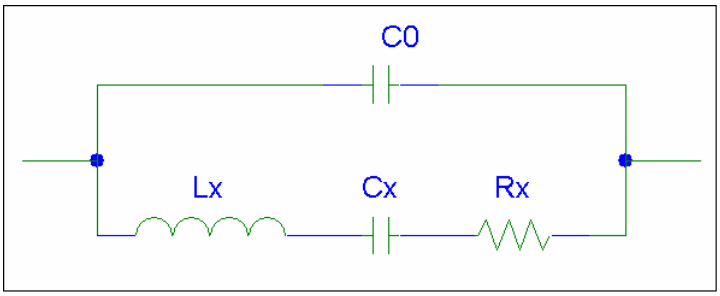

Fig. 4.2. Parasitic capacitance on top of resonating circuit

To see how parasitic capacitance affects the detection of resonance, we will have to look at the frequency response of such a circuit.

The impedance transfer function for the circuit represented in Fig. 4.2 can be derived as

$$impedance = \frac{s^2 L_x C_x + sR_x C_x + 1}{sC_x + sC_0\left(s^2 L_x C_x + sR_x C_x + 1\right)}$$

In MEMS capacitive devices, the input to the device is the potential V applied. Since current I is the desired output, the transfer function which we are interested in is

$$\frac{I}{V} = \frac{s^3 C_0 L_x C_x + s^2 C_0 R_x C_x + s\left(C_0 + C_x\right)}{s^2 L_x C_x + sR_x C_x + 1}$$

Assigning some arbitrary values to the model, letting

$$C_x = 32.5 \text{ pf}$$

$$R_x = 166\ \Omega$$

$$L_x = 0.29 \text{ mH}$$

will result in a resonating circuit of 1.8 MHz. The resultant bode diagram is plotted below (Fig. 4.3) for various orders of magnitude of parasitic capacitance. The legend shows the ratio of $\frac{C_0}{C_x}$.

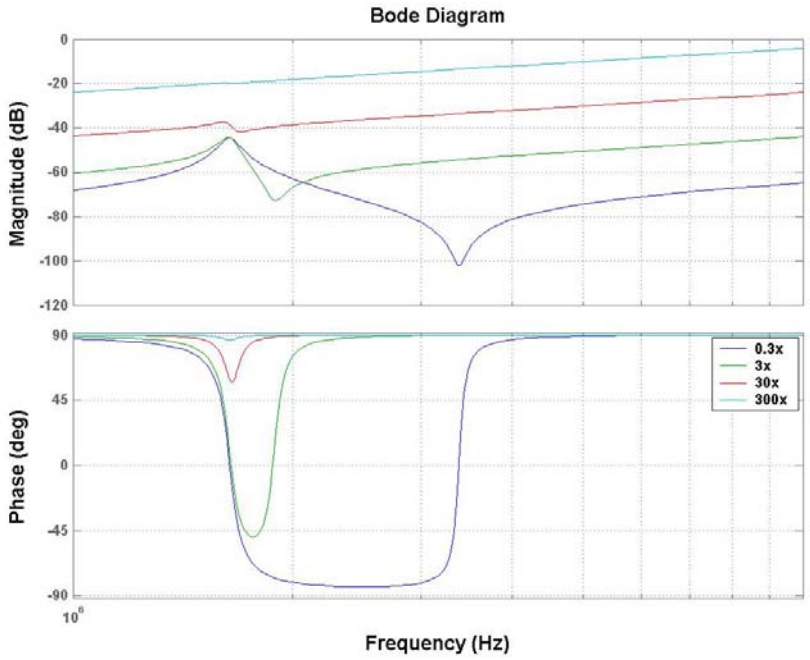

Fig. 4.3.Frequency response of resonating circuit with parasitics

As is evident from Fig. 4.3, the greater the parasitic capacitance values, the harder the detection of resonance of the circuit. At two orders of magnitude higher, the resonance peak will be practically undetectable.

What must be noted here at this time is that we are still dealing with linear elements. In reality, capacitive-based devices can be non-linear, and the non-linearity can be taken advantage of in the detection scheme. This will be discussed in Chapter 5, where a detection scheme utilizing such non-linearity is discussed.

4.4. Parameter Extraction

What has been discussed above is simply a means of representing mechanical characteristics in the electrical domain. This by itself does not seem to hold any purpose beyond the fact that the concept of parasitic capacitance is more easily visualized in the electrical domain. What will be further shown here is that if certain approximations are made, we are able to estimate the mechanical parameters from the electrical signals. This is done in a two-step process: first by analyzing the situation from a mechanical standpoint, and next, by looking at the electrical model and comparing the various terms involved.

From Chapter 2, we know that for parallel plate actuation, the capacitance relation is given by

$$C \approx \frac{\varepsilon A}{(d_0 - x)}$$

Therefore, the actuation force, given by $F = \frac{dE}{dx} = \frac{1}{2}\frac{dC}{dx}V^2$ is,

$$F = -\frac{1}{2}\frac{\varepsilon A}{(d_0 - x)^2}V^2$$

The negative sign suggests that the force is attractive.

Here, we will assume that the displacement of the plate, *x* is very small compared to the dimension of the gap, d_0, and therefore

$$F \approx -\frac{1}{2}\frac{\varepsilon A}{d_0^2}V^2 \qquad 4.2$$

Assume a configuration where the actuation is achieved through a DC with an AC voltage on top of it. As mentioned in Chapter 2, such a configuration will result in actuation at *w* as well as *2w* due to the non-linear relation in force. The actuation force at w is then

$$F \approx \frac{C_0 V_{DC}}{d_0}\hat{v}_{ac} \qquad 4.3$$

where $C_0 \approx \frac{\varepsilon A}{d_0}$ and $\hat{v}_{ac}$ is a phasor representation of the AC signal.

The solution for mechanical response, for the case of (4.1), is given by

$$\hat{x} = \frac{F/k}{1 - \frac{m}{k}w^2 + jw\frac{c}{k}} = \left(\frac{C_0 V_{DC}}{d_0 k}\right)\frac{\hat{v}_{ac}}{1 - \frac{w^2}{w_n^2} + j\frac{wc}{mw_n^2}} \qquad 4.4$$

The resultant current can be expressed as

$$i(t) = \frac{d}{dt}\left[C(t)v(t)\right] = C(t)\frac{dv(t)}{dt} + v(t)\frac{dC(t)}{dt} \approx C_0\dot{\hat{v}} + V_{DC}\frac{dC(t)}{dt}$$

or written in phasor form as

$$\hat{i} \approx jwC_0\hat{v}_{ac} + jwV_{DC}\left(\frac{C_0}{d_0}\right)\hat{x} \qquad 4.5$$

The first term on the right is due purely to parasitics. The second term is due to the vibration of the device, which is the component that contains the information that we want. The complete representation is:

$$\hat{i}_{mech} \approx jwV_{DC}\left(\frac{C_0}{d_0}\right)\left(\frac{C_0V_{DC}}{d_0k}\right)\frac{\hat{v}_{ac}}{1-\frac{w^2}{w_n^2}+j\frac{wc}{mw_n^2}} \qquad 4.6$$

Next, we look at the electrical model and attempt to draw a similarity. The current from the model can also be decomposed to two parts: one from the parasitic capacitance and the other from the resonator circuit. Since we are only interested in the current due to the resonating circuit, we can show that

$$\hat{i}_{res} = \frac{C_x jw}{1-w^2L_xC_x + jwR_xC_x}\hat{v}_{ac} \qquad 4.7$$

If we compare the terms, the numerator gives

$$C_x = \frac{C_0^2V_{DC}^2}{kd_0^2}$$

the imaginary portion of the denominator gives

$$R_x = \frac{cd_0^2}{C_0^2V_{DC}^2}$$

the real part of the denominator gives

$$L_x = \frac{md_0^2}{C_0^2V_{DC}^2}$$

and the quality factor is given by $Q = \frac{w_nL_x}{R_x}$.

As expected, each of the equivalent electrical parameters contain its corresponding equivalent mechanical term: C_x is a function of k (spring), R_x is a function of c (damper) and L_x is a function of m (mass). If the electrical parameters can be extracted, we can then obtain estimations of the mass, spring constant and damping ratio of the device.

As it turns out, that is possible if parasitics is low enough or negligible. The simplest electrical parameter to be extracted would be R_x. At resonance, L_x and C_x effectively cancel each other out. Thus, the real part of impedance at the resonant frequency will be equal to R_x.

By measuring the Q of resonance, we can obtain L_x through the relation $Q = \frac{w_n L_x}{R_x}$. On a similar basis, resonance frequency for an electrical circuit is given by $w_n^2 = \frac{1}{C_x L_x}$. Thus by knowing the resonant frequency and L_x previously, C_x can be extracted.

This means of approximating mechanical parameters rely on several assumptions. Firstly, resonance must be detectable at the driving frequency. This has the added implication that parasitics must be sufficiently low so as not to mask the resonating signal. This depends on the physical design of the device and the set-up to minimise parasitics. Second, the DC voltage must be higher than the AC signal. This situation is easily achieved. Thirdly, the actual displacement of the device is small compared to the physical gap of the plates (or combs for that matter). This is again dependent on the design of the device, an assumption more probably satisfied by parallel-plates than comb-drives. Small changes in displacement for parallel-plates results in capacitance change large enough for detection purposes. Comb-drives would require essentially larger displacements to achieve significant capacitance variation.

4.5. Higher DOFs

Thus far, only a 1-DOF model has been explored. Difficulty arises when higher DOFs or more complex structures are to be visualized in electrical domain. As an example, consider the case of a 2-DOF structure as depicted by Fig. 4.4.

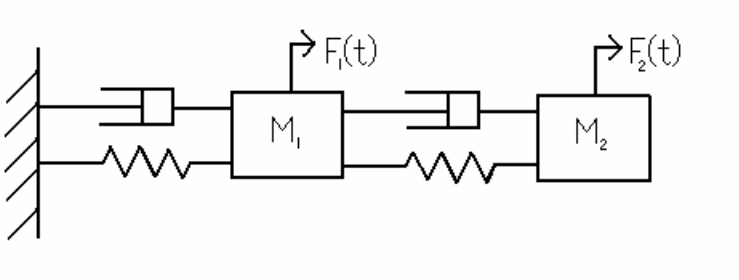

Fig. 4.4. 2-DOF mechanical resonating structure

On first glance, one may be tempted to suggest that the equivalent electrical model is two LCR circuits in series, i.e. as shown in Fig. 4.5.

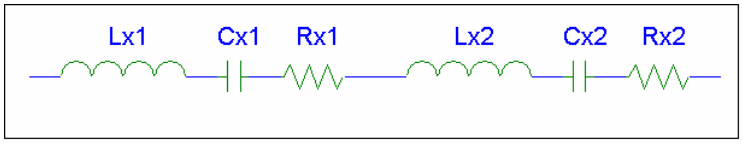

Fig. 4.5. Two LCR circuit in series

However, that is not the case. An obvious trait is to look at the 'flow' through all the elements in this model. In this case the *current* flowing through all the elements are equal. A 2-DOF mechanical model does not agree with this representation: the velocities experienced by each element need not be the same. This simple characteristic is sufficient proof that this is not the equivalent model we are looking for.

The next section shows how the equivalent electrical model can be obtained using Bond Graphs.

4.5.1. Bond Graph Conversion

As was mentioned earlier, Bond Graphs is a multi-domain representation method. As such, it should be expected that similar configurations in different domains have the same Bond Graph representation. This is the characteristic used to help us obtain the electrical model for higher DOF systems. We begin by looking at the 1-DOF system again.

For a 1-DOF mechanical system, the Bond Graph is given as Fig. 4.6.

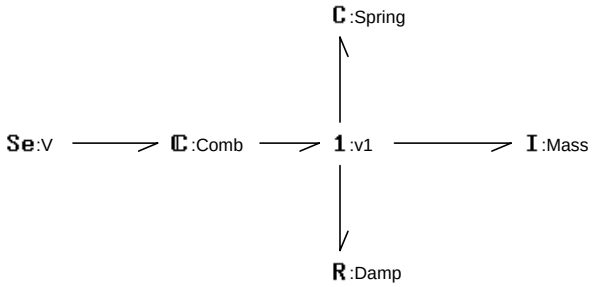

Fig. 4.6. Bond Graph model for a 1-DOF

The symbol (1) represents common flow junctions, which means that all the elements are experiencing an equal amount of flow, in this case velocity, in the system. The electrical model for a series LCR circuit has exactly the same representation, which tells us that the

equivalent model is exactly what we had obtained through the laborious process described earlier.

Now, looking at the 2-DOF mechanical model again, the Bond Graph can be shown to be as that in Fig. 4.7.

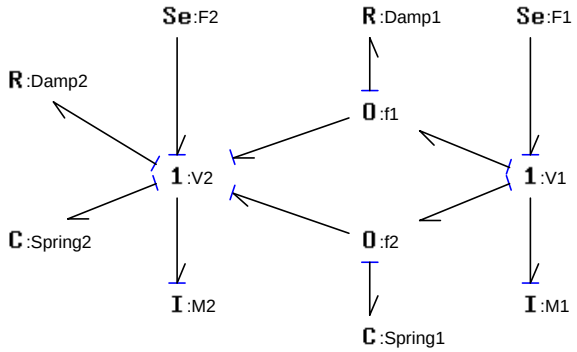

Fig. 4.7. 2-DOF Bond Graph model

It is not obvious in this case how the electrical model would look like, since it is always simpler to obtain the Bond Graph representation from a system than the other way round. However, by following some rules and recognizing the structural patterns involved, it is possible to reconstruct the electrical model.

One pattern that is immediately recognized lies on the left of Fig. 4.7. A termination of all the elements at a 1-node (common flow) will directly translate to a part of the circuit containing the elements in series. Other traits are not so obvious. One method would be to know what a standard configuration will translate to, and deduce from there. Two useful configurations are shown in Fig. 4.8

a).

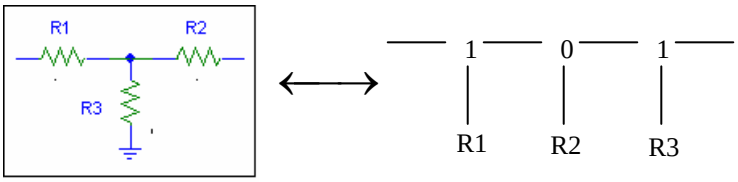

b).

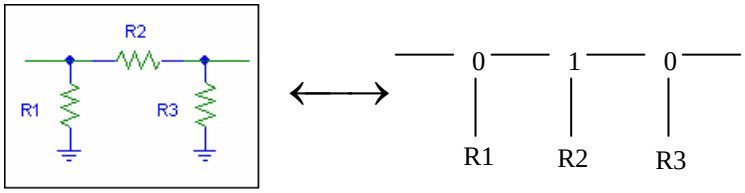

Looking at Fig. 4.7,

Fig. 4.8. Equivalent networked representations

configuration (a) fits the bill. A common effort node (0) is in between two common flow nodes (1). Putting things together, the equivalent 2-DOF model will be then as represented in Fig. 4.9.

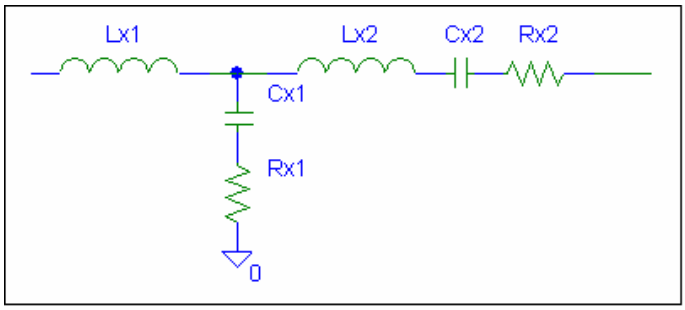

Fig. 4.9. Equivalent 2-DOF Electrical Model

The equivalent transfer function for such a circuitry is

$$\frac{I}{V} = \frac{s^3[C_1LC] + s^2[C_1RC] + s[C_1 + C]}{s^4[C_1L_1LC] + s^3[L_1C_1RC + R_1C_1RC] + s^2[L_1C_1 + L_1C + LC + R_1C_1RC] + s[R_1C_1 + RC] + 1}$$

Again, the transfer function is assigned some arbitrary values to show it is truly a 2-DOF model.

$$C = C_1 = 32.5 \text{ pf}$$

$$R = R_1 = 166\ \Omega$$

$$L = L_1 = 0.29 \text{ mH}$$

Fig. 4.10 shows the frequency response of such a system. As expected, the electrical circuit possess two resonance peaks.

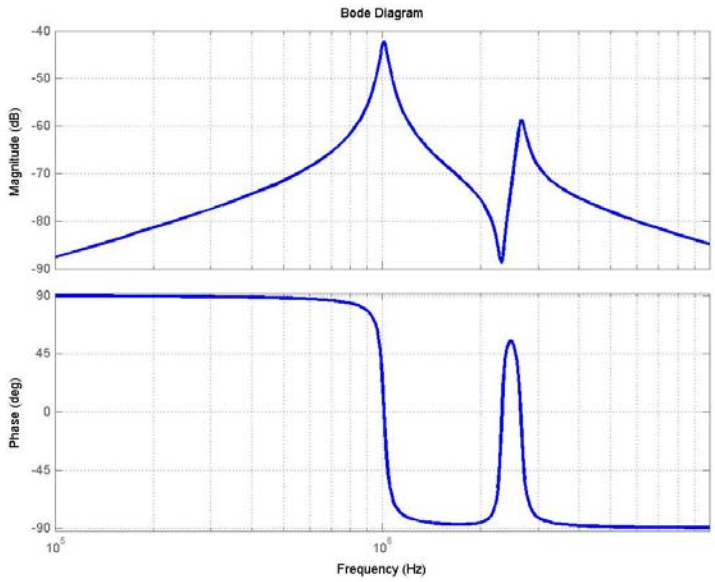

Fig. 4.10. Frequency response of obtained circuit

For more complicated structures, it is not a simple process to derive the electrical parameters and thereby estimate the mechanical parameters of the structure. However, the methodology has been demonstrated here, and it is a matter of application, depending on the structure that is being modelled.

As a further example, Clark et al [23] had demonstrated 2-DOF resonating structures. A simplified schematic is shown in Fig. 4.11 and the corresponding electrical equivalent model is shown in Fig. 4.12. The structure is made up of two resonators connected to each other through a beam (Fig. 4.11), modelled as a spring element.

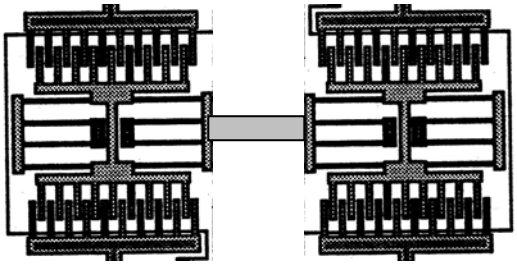

Fig. 4.11. Schematic of coupled resonators

If damping is neglected for the connecting beam, it is simply modelled as a capacitor in the electrical model (Fig. 4.12).

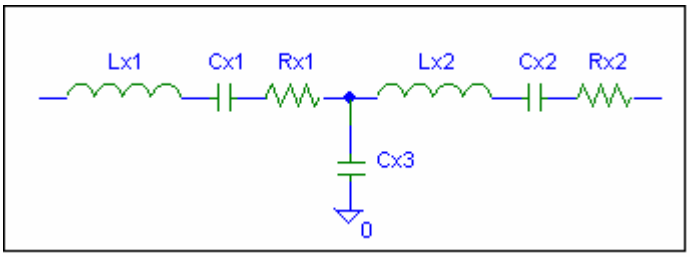

Fig. 4.12. Equivalent model for coupled resonators

4.6. Non-Linear Modelling

All the above modelling is only valid for linear elements. Unfortunately, as was shown in the previous chapter, MEMS parallel plate devices exhibit non-linear characteristics due to the V^2 term in the force. Moreover, in cases where miniaturization holds greater importance than easy detection, smaller devices means smaller capacitance changes and therefore are more susceptible to parasitics. In such cases, the detection scheme can rely on utilizing the characteristics of non-linearity to overcome the problem. This is discussed in the next chapter.

CHAPTER 5: Device Characterization

5.1. Initial Characterization

As shown earlier in Chapter 3, a parametric amplification system requires the device to be pumped at resonance to obtain maximum power transfer to the output. This knowledge is also necessary to design the filters for the input and output signals. However, the detection of resonance is not a straightforward process. As mentioned in the previous chapter, the existence of parasitic capacitance at an order of magnitude higher than the signal greatly complicates the detection.

As a result, it had been necessary to circumvent the problem through the use of techniques such as Electrical Amplitude Modulation (EAM) [18] as well as *2f* detection [17]. However, these methods have a severe limitation: implementation is possible only for two-port devices. Take, for example, the *2f* technique applied to a resonator (Fig. 5.1).

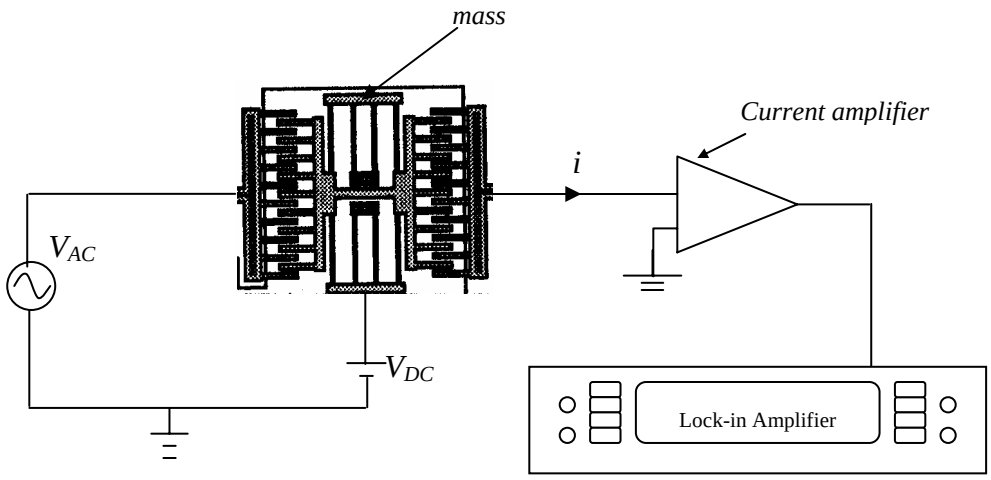

Fig. 5.1. Schematic for *2f* resonance detection scheme

The excitation of the device is achieved through the pumping of an AC signal on one side of the combs, with a DC voltage applied to the mass. As shown in Chapter 2, such a configuration results in the device resonating at the frequency *w* of the AC as well as at *2w*. The other side of the comb is then connected to a current amplifier, which will then be at virtual ground. A current, *i(t)* results at the comb due to the capacitance variation and the presence of the DC voltage. Detection is done not at the pumping

frequency *w* but rather at *2w* as the current due to parasitics occurs solely at *w*. Thus the need for a lock-in amplifier to do the signal processing.

In summary, these methods require one port for actuation and the other port for detection of the signal. Such schemes are not applicable for one-port devices. To the author's knowledge, there is no method which is suitable for one-port devices.

A simple alternative is proposed here: to send an AC signal into one side of the plate only. The AC input will contribute in two ways: it actuates the one-port device as well as modulates the detected signal. With just an AC, the actuation force occurs singly at *2w* only. In this chapter, a modified *2f* detection, termed *3f* detection, is presented and analyzed. Before this *3f* detection scheme is discussed, we first introduce an instrument that is essential to this technique: a Lock-In amplifier.

5.2. Resonance Detection

Raskin et al. [12] detected resonance for their parallel plate device by applying AC on top of a DC on one plate and a current amplifier to the other. The situation may be represented as:

$$v(t) = V_{ac}\sin(wt + \phi_1) + V_{dc}$$

and

$$C(t) = C_0 + C_w \sin(wt + \phi_1) + C_{2w}\sin(2wt + \phi_2)$$

We can show that there are effectively three frequencies which we can detect at. We know that

$$i(t) = \frac{d}{dt}[C(t)v(t)] = C(t)\frac{dv(t)}{dt} + v(t)\frac{dC(t)}{dt}$$

The current output at frequency *w*:

$$C_0 wV_{ac}\cos wt - \frac{1}{2}wV_{ac}C_{2w}\sin(wt + \phi_2) + \frac{1}{2}wV_{dc}C_w\cos(wt + \phi_1)$$

2w:

$$wV_{ac}C_w\sin(2wt + \phi_1) + 2wV_{dc}C_{2w}\cos(2wt + \phi_2)$$

3w:

$$\frac{3}{2}wV_{ac}C_{2w}\sin(3wt + \phi_2)$$

For Raskin et al, parasitic capacitance is not much of an issue as their capacitance change for the membrane is in the order of 100-600 pf. With actuation force for a DC and AC combination contributing to actuation frequencies at *w* as well as *2w*, they could detect resonance at *w*. Such a direct measurement is only possible if the capacitance change is significantly larger (by an order of magnitude) than the amount of parasitics.

However, in our case, the aim is to demonstrate parametric amplification for small capacitance devices. At such scale, the average device has only a few picofarads of capacitance with capacitance change in the range of around tenths of picofarads. The presence of parasitics at even 10 pf is sufficiently large to conceal the signal at *w*.

5.3. Lock-in Amplifier

The detection of resonance is not possible at the driving frequency but at higher multiples of the input signal. To obtain the frequency response curve for such a system, we use a lock-in amplifier with a current amplifier as our detection scheme.

Lock-in amplifiers are used to detect and measure very small AC signals. The principle of operation is based essentially on the mathematical relation that

$$A\sin(w_1 t)\sin(w_2 t) = \frac{A}{2}\left[\cos(w_1 - w_2)t - \cos(w_1 + w_2)t\right]$$

where w_1 and w_2 represents some arbitrary frequencies and A represents an arbitrary constant which is the magnitude of the signal we want to detect.

If $w_1 = w_2$, then we see that the first term on the right reduces to a constant. This constant contains the magnitude of the signal we are interested in. Thus, by sending the resulting signal through a low pass filter to remove all frequency signals, we can obtain the magnitude of the signal which would otherwise be overwhelmed by noise or stray signals.

This simple mathematical relation results in a highly versatile instrument that allows the user to either extract a signal within a very noisy environment or make high-resolution measurements. The lock-in amplifier requires a reference signal to do the internal multiplication. Typically, the device is excited at a certain frequency, and this excitation can be external or from the lock-in amplifier itself. The output signal is fed into the instrument and based on the reference (the external excitation or its own output

signal), internal processing is done to extract the signal occurring at that reference frequency.

By repeating this process for a range of frequencies, and extracting the DC component every time, we effectively get the frequency response of the device. The lock-in amplifier basically sweeps through the frequency range and does an internal multiplication of the received signal. The input signal is multiplied at the driving phase as well as at 90° phase shift. So the user is able to plot frequency response curves at X (0°) and Y (90°) against frequency as well as magnitude $\left(\sqrt{X^2+Y^2}\right)$. The phase relation is obtained through $\tan^{-1}\left(\frac{Y}{X}\right)$ at each frequency point.

The 'quality' of the extracted signal depends upon several factors, amongst which is naturally the passband of the lowpass filter. The smaller the passband, the closer we get to obtaining purely the DC signal. However, since the filters used are digital filters, it also means that a longer sampling time is required for tighter passbands. For a digital lock-in amplifier (which is what is being used), another factor would be the user-defined sensitivity. Since the number of bits in the internal memory is fixed, by stating the value of the maximum voltage that can be measured, the resolution of the readings is affected as well. If the maximum voltage is stated too high, small fluctuations in the signal will not be extracted. In essence, careful control of the various parameters in a lock-in amplifier has to be observed to extract the embedded signal properly.

More detailed operation and characteristics of lock-in amplifiers can be found in ref [17].

5.4. 3f Detection Scheme

The reference frequency that is multiplied internally by the lock-in amplifier need not be at the driving frequency. It can also be at multiples of the driving frequency. That is the basis of the *2f* measurement technique. Parasitic capacitance only affects the signal at the driving frequency and capacitance variation also occurs at two times the driving frequency. Therefore, the frequency response of the device can be obtained by using the lock-in amplifier to detect at twice the driving frequency.

Using a *3f* measurement to detect resonance, we apply a single V_{ac} to one side of the device and the current amplifier to the mass. We now derive the exact output relation. For an input of $V = V_{ac} \sin wt$, the actuation force is affected by the term V^2

$$V^2 = (V_{ac} \sin wt)^2 = V_{ac}^2 \frac{1}{2}(1 - \cos 2wt)$$

To simplify our analysis later, we re-write the above equation as $\sin\left(2wt - \frac{\pi}{2}\right) = -\cos 2wt$, resulting in

$$V^2 = V_{ac}^2 \frac{1}{2}\left(1 + \sin\left(2wt - \frac{\pi}{2}\right)\right)$$

From mechanical vibration, we know that for an excitation force of $F = F_0 \sin w_d t$ where w_d is the applied driving frequency, the resultant response is given by

$$x = X \sin(w_d t - \phi)$$

where $X = \dfrac{\frac{F_0}{k}}{\sqrt{\left(1 - \frac{m{w_d}^2}{k}\right)^2 + \left(\frac{cw_d}{k}\right)^2}}$

and $\tan\phi = \dfrac{\left(\frac{cw_d}{k}\right)}{1 - \frac{mw_d^2}{k}}$

Similarly, the resultant capacitance change must approximately be of the form,

$$C(t) = C_0 + 2\gamma_1 C_0 \sin\left(2wt - \frac{\pi}{2} - \phi\right)$$

where ϕ is a function of driving frequency and $\phi = \frac{\pi}{2}$ at resonance. (This is not exactly true since the actuation force is actually non-linear, as it is a function of displacement as well. However, it can be shown that the resultant excitation at *w* is sufficiently small to be neglected). γ_1, defined in this case, is the term that varies with the frequency and the V_{ac} applied to the device. Naturally, γ_1 will be greatest at resonance for a given V_{ac}.

Now, we want to see the current output phase relations. As usual, we use

$$i(t) = C(t)\frac{dv(t)}{dt} + v(t)\frac{dC(t)}{dt}$$

For this configuration, the resultant current output is

$$i(t) = C_0 wV_{ac}\cos wt - \gamma_1 C_0 wV_{ac}\sin\left(wt - \frac{\pi}{2} - \phi\right) + 3w\gamma_1 C_0 V_{ac}\sin\left(3wt - \frac{\pi}{2} - \phi\right) \quad 5.1$$

Detecting resonance at *3f*, we are effectively detecting the third term.

Therefore, the device is resonating at *twice* the driving frequency, but the detection is done at *thrice* that frequency. The lock-in amplifier effectively plots the response curve with the x-axis being the value of the driving frequency. So, to interpret the plot, i.e. to obtain the actual frequency response of the device, one needs to multiply the x-axis by a factor of 2.

Essentially, that single AC input into the device performs two functions. Firstly, it actuates the device at twice the input frequency. Secondly, it performs an amplitude modulation on the output signal at the same time. The relevant signal to be extracted then exist at three times the input frequency.

Detecting resonance is not straightforward. There may be multiple little peaks due to irregularities when the initial broad frequency sweep is done. The highest peak is naturally taken to be resonance. However, the phase and X, Y plots allow us to verify resonance with greater confidence.

For this 3f detection scheme, resonance is confirmed upon seeing an 'inverted' peak for X and a 'S' on its side for Y. Our interest is in the term $3w\gamma_1 C_0 V_{ac}\sin\left(3wt - \frac{\pi}{2} - \phi\right)$. Vibration analysis tells us that $\phi = \frac{\pi}{2}$, so the net phase change in the signal is $-\pi$.

5.5. Extraction of γ_n coefficients

From the derivation of parametric amplification in Chapter 2, knowledge of the various γ_n coefficients is necessary to estimate the characteristics of the parametric device. In this section, we will discuss the means of extraction.

γ_n is effectively the value of the capacitance change ratio at the resonating frequency. As such, there is no direct means of obtaining it. Some indirect method has to be used. Since current is the most easily obtainable output which can be measured, it is natural that it be examined first. Looking at

$$i(t) = \frac{d}{dt}\left[C(t)v(t)\right] = C(t)\frac{dv(t)}{dt} + v(t)\frac{dC(t)}{dt} \qquad 5.2$$

a possible method of extracting the coefficients would be to obtain capacitance-time, *C(t)* and then obtain the various coefficients by some means of fourier transform. Rearranging (5.2) the capacitance time information can be obtained through

$$C(t) = \frac{\int i(t)dt}{v(t)}$$

The capacitance change can be approximated to be,

$$C(t) = C_0 + \sum 2\gamma_n C_0 \cos\left(w_n t + \phi_n\right)$$

or

$$C(t) = C_0 + \sum 2\gamma_{nc} \cos(w_n t) + \sum 2\gamma_{ns} \sin(w_n t)$$

taking as many terms as necessary. Knowing *C(t)*, we can extract each of the coefficients. Since $R\cos(a+b) = R\cos a\cos b - R\sin a\sin b$, to obtain γ_n and ϕ would then be

$$\gamma_n = \sqrt{\gamma_{nc}^2 + \gamma_{ns}^2}$$

$$\varphi = \tan^{-1}\left(-\frac{\gamma_{ns}}{\gamma_{nc}}\right)$$

However, this approach did not work out for two main reasons. Firstly, *i(t)* data obtained from the oscilloscope are found to contain too much noise (Fig. 5.2). As a result, the processed $Q(t) = \int i(t)dt$ fluctuates too much. An example of the processed *Q(t)* is shown in Fig. 5.3. There seems to be a bias in the current, which should not be due to the purely sinusoidal input. This bias, attributed mostly to noise, explains why the *Q(t)* (Fig. 5.3) increases with time.

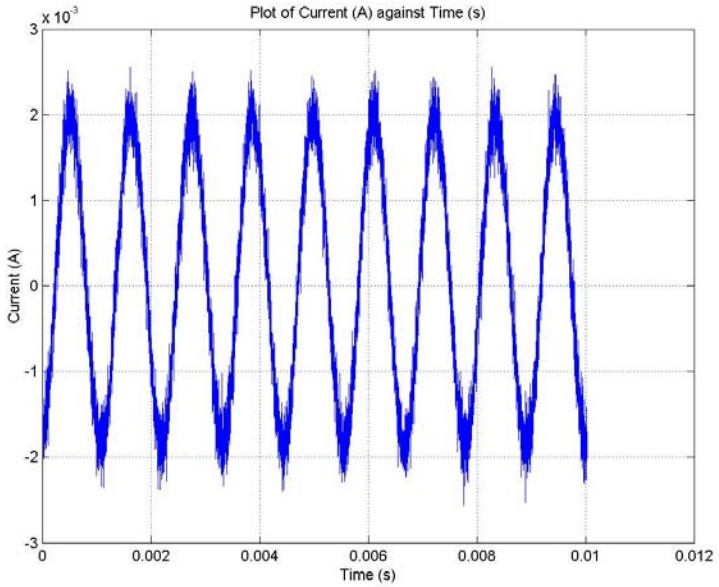

Fig. 5.2. Plot of extracted noisy current against time

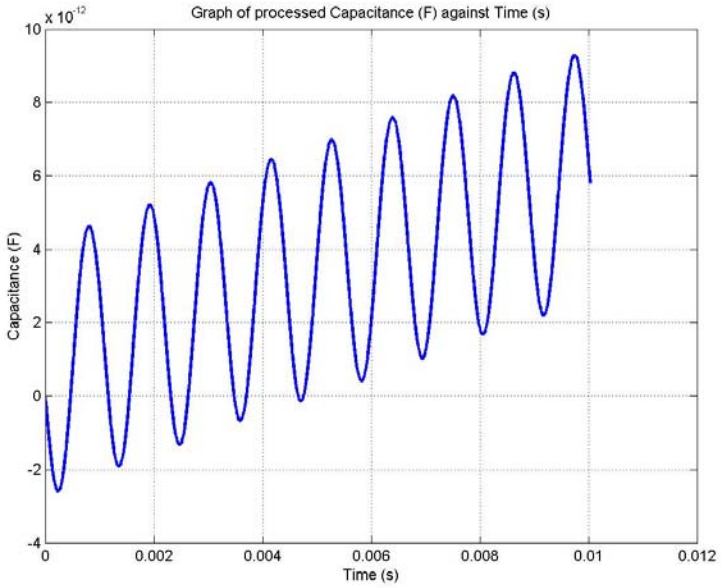

Fig. 5.3. Plot of processed *Q(t)*

Secondly, as only an AC signal is applied, there are values for which $v(t) = 0$. This will result in situation where a division by zero needs to be done and therefore such a method is not applicable.

This problem can be solved if the actuation port has a DC bias larger than the AC signal, which would remove such zero potential points. However, a DC bias will shift the equilibrium position of the device. The practical set up of a parametric amplification do not actually require a DC bias applied to the system. Moreover, the bandpass filters required in the set up will not allow the DC signal to reach the device. As such, this operation to obtain γ_n is unrealistic since we may be able to extract γ_1 at the end but at a mode of operation unreflective of the actual final set up.

As a result, the problem has to be approached in another manner. Since we are only concerned with the coefficients γ_n, we can avoid the impasse if we do not need to use the full waveform of *C(t)*. We know that current can be approximated by (5.1)

$$i(t) = C_0 w V_{ac} \cos wt - \gamma_1 C_0 w V_{ac} \sin\left(wt - \frac{\pi}{2} - \phi\right) + 3w\gamma_1 C_0 V_{ac} \sin\left(3wt - \frac{\pi}{2} - \phi\right)$$

The value of γ_n is actually contained in the coefficient of *3w*. Thus, by extracting the coefficients directly from the sampled *i(t)*, we can obtain the value of γ_n.

5.5.1 Extraction method

Fourier analysis does not give the actual amplitude of the embedded signal of the frequency. Instead, the magnitude shown is usually at some arbitrary scale, with the intent of showing the 'strength' of the signal. Some modifications of the fourier transform would thus be necessary to apply it in our case. Fig. 5.4. visualizes the operation.

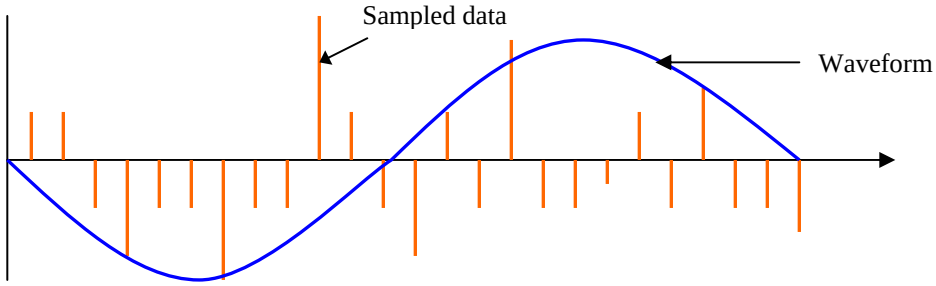

Fig. 5.4. Sample data multiplied by a sinusoidal waveform

The basis of fourier analysis lies in the fact that we can know the strength of the signal at a certain frequency if we multiply it by a series of weights, which approximates a sine or cosine wave. By summing the result for that frequency sampled, the larger the

value of the output the stronger the presence of that frequency. On the other hand, the sum will be close to zero if the sample does not contain the frequency of the wave: the positive values will approximately cancel out the negative values. If we were to vary the frequency of the sine or cosine wave and multiply them with the sampled data, we effectively obtain a plot or *frequency spectrum* showing the various strengths of the sampled data at different frequencies.

Since the resulting value for a correlated frequency gets larger as the time sampled increases, it also explains why resolution improves for longer sampling time for fourier transform.

In our case then, the magnitude of the resultant summed weights cannot allowed to be arbitrary. A sampled sine signal of, say, $3\sin wt$ must give a result of a value 3. To do that, we have to do some form of compensation to the weights.

It is perhaps easier to find the solution to the problem by looking at a perfectly correlated sampled data of the function $\sin wt$. Now, if the waveform used is also $\sin wt$, the resulting summed value will be $\sum(\sin wt)^2$. The exact value of $\sum(\sin wt)^2$ depends on two factors: the sampling rate (which will determine how many values are taken within a period of time) and the sampling time. It is easily seen then that the higher or longer either of these factors is, the greater the magnitude of the result.

The solution should now seem obvious: simply divide every waveform result by its magnitude squared i.e. ($\sum(\sin nwt)^2$) to normalize the value to 1. Take for example the case above. If the sampled data is of the function $3\sin wt$, the resultant summed weights for a waveform of $\sin wt$ will be $\sum 3\sin wt \times \sin wt = 3\sum(\sin wt)^2$. Thus by dividing the result by the squared sum of the waveform, $\sum(\sin wt)^2$, we extract the magnitude 3.

So, by dividing the value obtained for a sampled sine wave of magnitude 1, we will normalize the value to 1 and obtain the value of the coefficient exactly, i.e.

$$\gamma_{ns} = \frac{\sum current \times \sin(nwt)}{\sum(\sin nwt)^2} \qquad 5.3$$

$$\gamma_{nc} = \frac{\sum current \times \cos(nwt)}{\sum (\cos nwt)^2} \qquad 5.4$$

As mentioned earlier, $\gamma_n = \sqrt{\gamma_{nc}^2 + \gamma_{ns}^2}$.

After extracting $\gamma_n = 3w\gamma_1 C_0 V_{ac}$, γ_1 can be obtained by dividing by the various terms in the expression. However, it must be acknowledged here that this method to extract coefficients will result in approximate values.

5.6. Extracting R_c

It is necessary to obtain the internal resistance, R_c of the device. R_c will determine the amount of internal losses of the device. Simply by applying a voltage across the terminals and measuring the resulting output will not work in this case since we are actually measuring a variable capacitor.

From the previous chapter, it is recognized that a resonating device can be represented as a series LCR with a parasitic capacitance C_0 in parallel. A model which includes the internal resistance of the device, R_c, the equivalent circuit would be depicted as in Fig. 5.5.

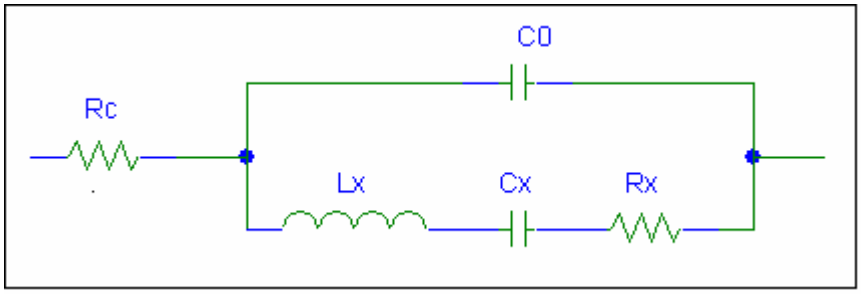

Fig. 5.5. Equivalent electrical model of device

The equivalent impedance can be derived from the circuit representation to be

$$imp_{eff} = R_c + \frac{jwR_xC_x + \left(1 - w^2L_xC_x\right)}{jwC_x + jwC_0\left(jwR_xC_x + 1 - w^2L_xC_x\right)} \qquad 5.5$$

Simply by observation, it can be seen that resonating the device at high frequencies will result in the second term being equal to zero, thereby obtaining

$$imp_{eff} \approx R_c$$

The internal resistance of the device can subsequently be determined.

In mechanical terms, driving the structure at frequencies beyond its natural frequencies results in amplitudes of vibration approaching zero. The structure then approaches a system of a fixed capacitor. The resistive parameter of the device is then measurable.

CHAPTER 6: Filter Design

6.1. Filter Design

Filter design is a very mature field [24], so not much discussion will be done here. A general comparison of the performance of each type is given below [25]:

Butterworth: flat pass band, adequate roll-off, mathematically simpler

Chebyshev: steeper roll-off, greater pass-band ripple

Elliptic-function: equal-ripple variation in both passband and stopband

In this project, the aim is to verify parametric amplification in MEMS devices. Though the use of transistors in the circuitry actually introduces additional shot noise into the system, the noise analysis is not within the intended scope of the project. The use of active filters will greatly simplify the design and testing of the circuitry since the load does not have to be considered during the design of the filters.

6.1.1 Active filters

The design of active filters lies in the topology of the various ‘op-amps’, capacitors and resistors. There are many configurations of such topologies, most of them having second order transfer functions. The term ‘biquad’ refers to these configurations. Knowing the final transfer function that is required, it is simply a matter of breaking down the transfer function into various second order fractions, each of them realized using a biquad and finally cascading them together to form the final filter.

A Kerwin-Huelsman-Newcomb (KHN) second order biquad was one of first such designs based on the state-variable method. The circuit consists of three connected op amps. The first implements a differential summer and the next two are inverting integrators. Fig. 6.1 shows the circuit layout for the biquad.

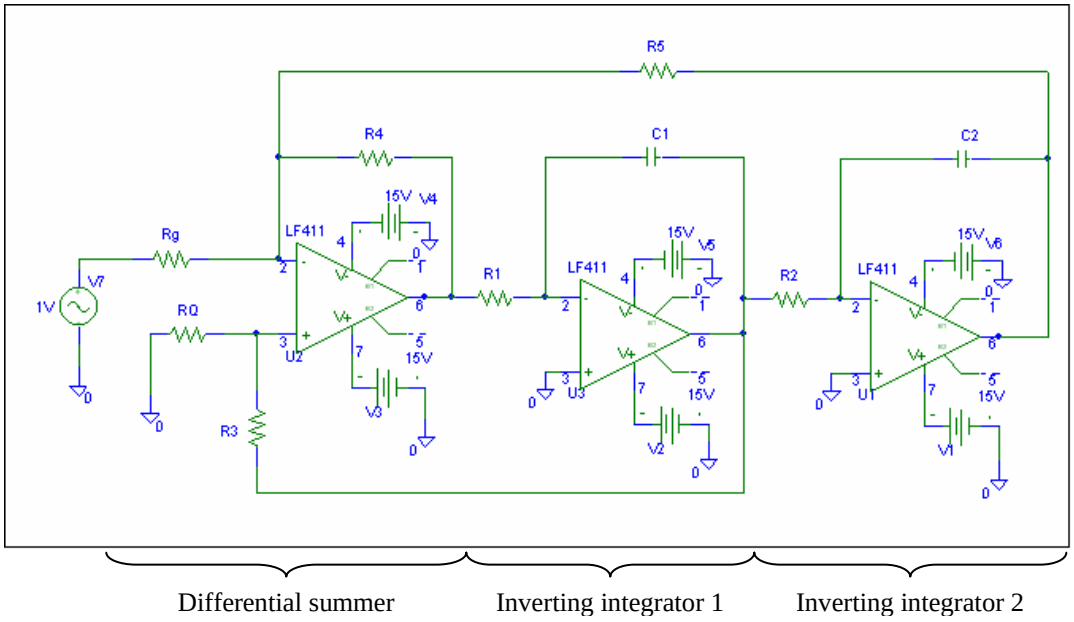

Fig. 6.1. Schematic for a KHN biquad

Depending upon which output of the op-amp you tap out, you can realize a low-pass, high-pass or band-pass filter: the output from the differential summer will result in a high-pass filter, a band-pass filter if tapping from inverting integrator 1 and finally a low-pass filter from inverting integrator 2.

The transfer function for a second order band-pass configuration can be derived and shown as

$$\frac{V_0}{V_s} = \frac{s\dfrac{R_4 R_Q (R_5 + R_6)}{R_1 R_5 R_{set} C_1}}{s^2 + s\dfrac{R_G R_Q (R_5 + R_6)}{R_1 R_5 R_{set} C_1} + \dfrac{R_6}{R_1 R_2 R_5 C_1 C_2}} \qquad 6.1$$

The filter characteristics that can be expressed are given below [33]

$$w_n^2 = \frac{R_4}{R_5 R_1 R_2 C_1 C_2} \qquad 6.2$$

$$Q = \frac{1 + \dfrac{R_3 (R_G + R_Q)}{R_G R_Q}}{1 + \dfrac{R_4}{R_5}} \left(\frac{R_4 R_1 C_1}{R_5 R_2 C_2} \right)^{\frac{1}{2}} \qquad 6.3$$

$$gain_{BP} = \frac{R_3}{R_G} \qquad 6.4$$

This implementation is easily achieved through the use of Burr-Brown's UAF42 Universal Active Filter IC [32]. It is a 14-pin DIP (Dual Inline Package), which comprises of four op-amps and certain fixed capacitance and resistance values. Three of the op-amps are wired internally as a KHN biquad, with the last one separated from the rest of the circuit to be used as an inverter or a tuned circuit. With $R_4 = R_5 = R_3 = R_G = 50k\Omega$ and $C_1 = C_2 = 1000pF$ fixed internally in the IC, we have R_1, R_2 and R_Q to vary to achieve the desired characteristics. The pins layout is shown in Fig. 6.2. The IC requires two power inputs, V+ and V-. The power supply required is about +15 V and –15 V respectively. A ground connection is also required for the IC (pin 11).

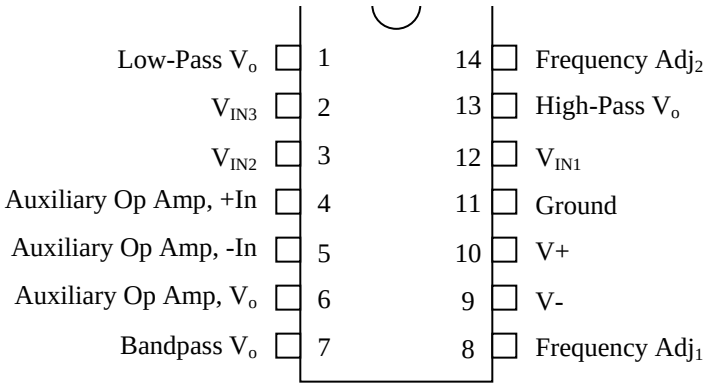

Fig. 6.2. Schematic of pins layout

Design of the filter is then varying R_1, R_2 and R_Q to suit the characteristics. Burr-Brown provides a series of FilterPro^{TM} computer-aided design programs to guide the user through the design process. The program contains a library of commercially available resistance values. By designating the desired filter characteristics, the program searches through its database and comes up with the resistor values which best matches the performance required. A sample program screen is shown in Fig. 6.3.

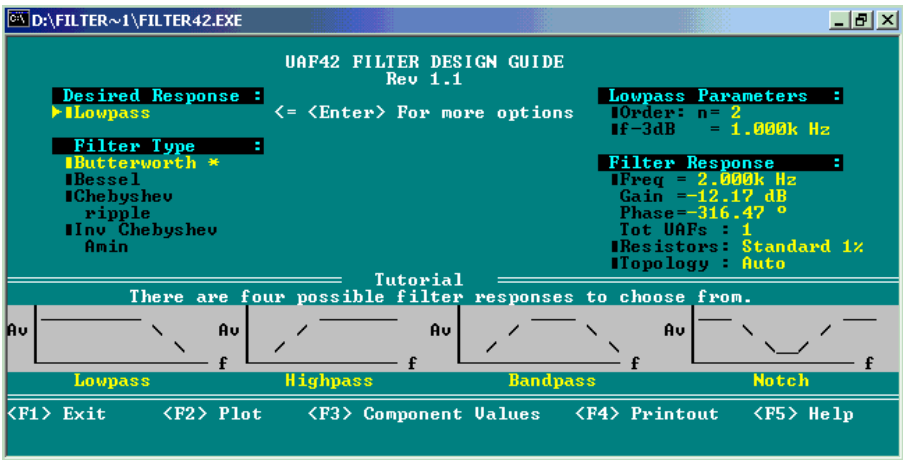

Fig. 6.3. Sample screen shot of FilterPro program

6.2. PCB Design

As noted earlier, the effect of parasitics poses problems in the detection of MEMS devices. Imperfect connections, haphazard wiring all may result in contamination of the signals. Thus, in the implementation, a generic PCB was designed instead of using normal boards. This reduces the amount of soldering, connections and possible improper connecting wiring. It was foreseen that the maximum number of cascaded stages of filters is three, due to the fact that the greater the number of stages, the greater the amount of insertion losses. The PCB was drawn using Protel™ [31] and sent for fabrication at EDA Singapore. The drawn PCB is shown in Fig. 6.4.

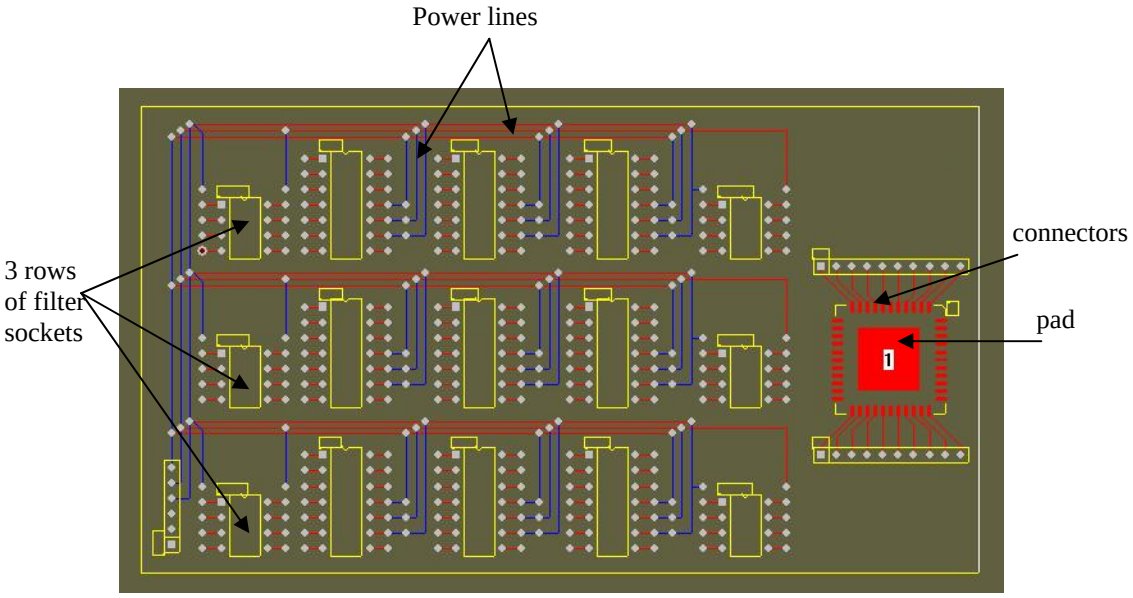

Fig. 6.4. Drawing of PCB in Protel

The PCB was designed to be as generic as possible. It is a two-layer board: the lines in red at the top layer and the lines in blue the bottom layer. There are three rows of ICs intended for the three filters that are required. Three lines of power are supplied to the chips: one line for ground, another for +15V and the last for –15V, which are the operating voltages of the ICs. Though not marked on the drawing, the ground wirings run in between the +15 V and –15 V supply (the middle line of the three lines) to minimize stray electric fields on the board. This is intended to reduce parasitics.

The pad on the right (Fig. 6.4) is meant for cases in which the device is not packaged. The die can then be fixed there and connections wire-bonded to the connectors.

The 8-pin DIPs are included on the board to accommodate possible future generic op-amp ICs.

CHAPTER 7: Experiment Results

7.1. Device Selection

The device to be used to verify parametric amplification is chosen based on several criteria. From the theoretical result, we know the importance of the following:

- High resonant frequency

We know that the amplification factor depends largely on the frequency ratios for an up-converter. So higher resonant frequencies for the device will result in greater gain. At the same time, the required filter will not need a steep cut-off, reducing the order of the design. To implement parametric amplifiers practically, the frequency of the signal to be amplified may not be low, perhaps of the order of kHz or MHz. In this case, to get substantial amplification, we will require the device to be operating at the MHz or GHz range. All these issues constitute the necessity for high resonant frequency devices.

Among the parameters which affect effective impedances of the up-converter, the operating frequencies and C_0 has the greatest variation. Operating at high frequencies will allow the effective input and output impedances to be low, which may or may not be a necessity for the operation.

- High capacitance change, γ_n

In a similar fashion, the amplification depends practically on the amount of capacitance change in the device. In the choice of the device to use, it is preferable that γ_n can be varied substantially so that γ_n dependence can be demonstrated. Unfortunately, there is no direct means of measuring γ_n.

- Low resistance

Naturally, it is favourable for the resistance of the device to be as small as possible to minimize losses. On the other hand, in the application of degenerate amplification, the presence of real losses in the device might be useful to stabilize the system.

- Low average capacitance, C_0

C_0 encompasses mainly parasitic capacitance as well as the average capacitance value. We would want parasitics to be as low as possible as they affect the actual operation of the device as well as hinder the accurate detection of signals.

In view of these selection criteria, the resonant frequency of the device was decided to be of higher importance and the simplest to select. Among the various accelerometers and gyroscopes tested that contain a parallel plate mechanism, a BARS gyroscope [27] was finally chosen. Initial testing in air showed a resonance frequency at ~1800 Hz at the sensing side, which is the highest among the various devices available. The results are shown in the next section.

Moreover, the amount of capacitance variation of the BARS gyroscope is large with a range of ~0.2 pf, compared to other devices. Among the devices tested for suitability were some MUMPs accelerometers and EG&G accelerometers. However, they were found to be unsuitable for various reasons: low resonance frequency, trapped charges, low pull-in voltage, etc.

7.1.1 BARS Gyroscope

Basically, the gyroscope comprises an actuation side and a sensing side. The actuation combs consist of comb-drives for the purpose of providing a constant actuation force. The sensing plates are parallel-plates, meant for larger capacitance variation and therefore the side suitable for our use. Fig. 7.1 shows an SEM of the BARS gyroscope used.

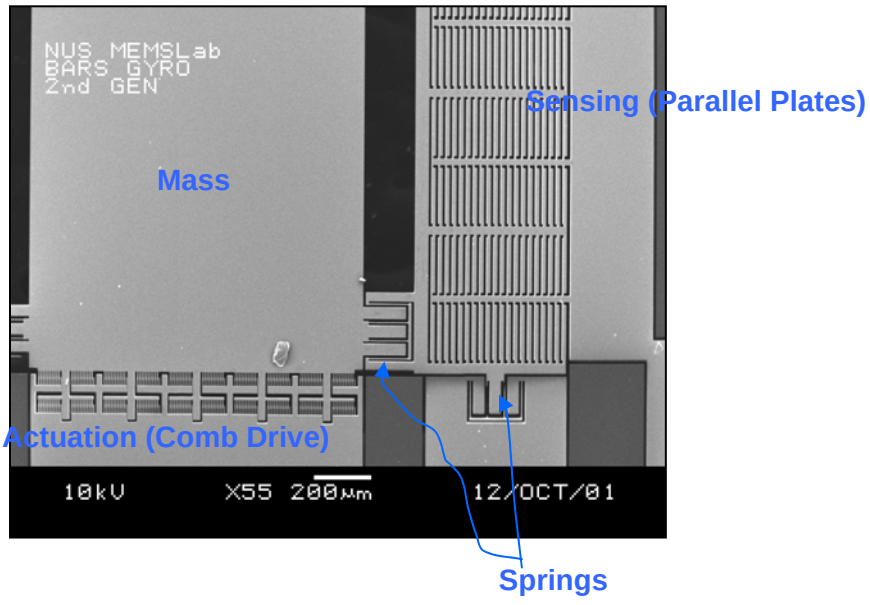

Fig. 7.1. SEM of BARS gyroscope

The device is packaged on a 24-pin DIP (Dual Inline Package). The pins configuration is shown in the Table 7.1.

Table 7.1: Pins layout of device

Name	Pin Number
Ground	16
Mass	14
Actuating 1	20
Actuating 2	12
Sensing 1	18
Sensing 2	10

7.2. 3f Detection results

The resonant frequency of the device is the first thing that must be determined. The *3f* detection scheme described in Chapter 5 was used for this purpose. The device resonance is tested on both sides of the device. Port 14 of the device connects to the mass; ports 10 and 18 are the two parallel plates. The schematic of the measurement setup is shown in Fig. 7.2.

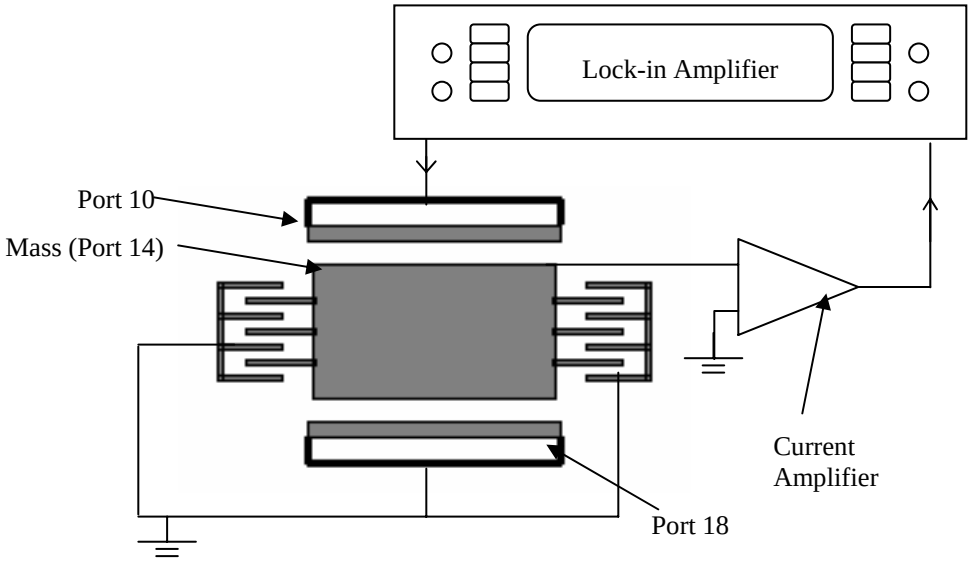

Fig. 7.2. Schematic of the 3f measurement setup

The graphs below show the results obtained at atmospheric pressure. Measurements were done between port 10-14 as well as 18-14.

7.2.1 Results for port 10-14

The result is shown in Fig. 7.3. The characteristic of the 3f detection scheme is the inverted peak for X and the slanted 'S' for Y, as seen in the plot. As mentioned in Chapter 5, section 5.4, the true frequency response of the device is two times what the x-axis shows. In this case, since Y cuts at about 900 Hz, the resonance in air about 1800 Hz.

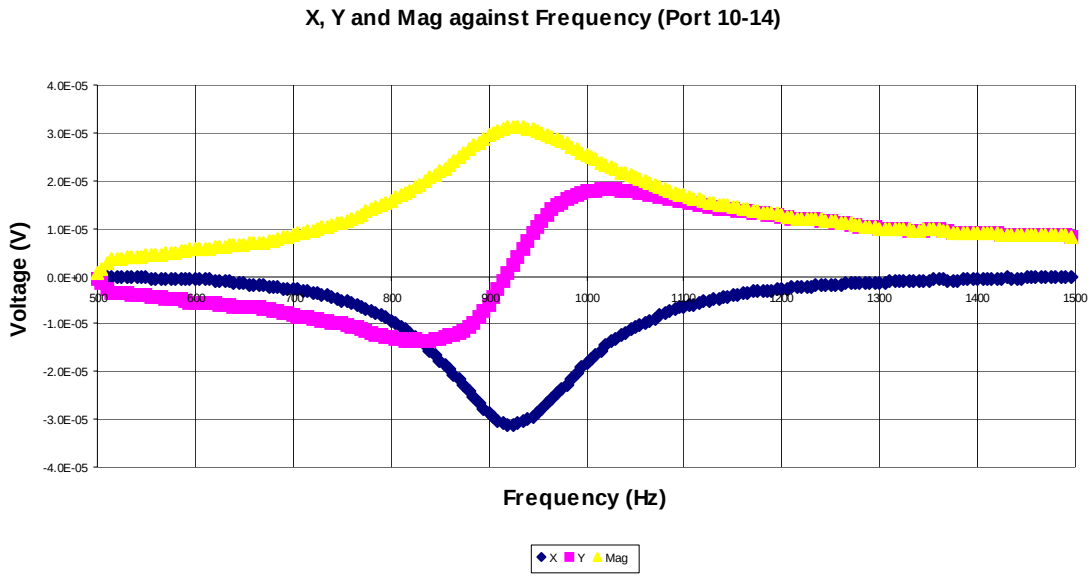

Fig.7.3. 3f detection for port 10-14

7.2.2 Results for port 18-14

Fig. 7.4 shows the result for port 18-14. As expected, the resonance is also about 1800 Hz (after multiplying the x-axis frequency by two).

As can be seen, the resonance in air is about 1800 Hz. With that in mind, the required filter for the pump will be one at half the resonance (because the excitation will be at twice the pump frequency without a DC bias), i.e. one at 900 Hz.

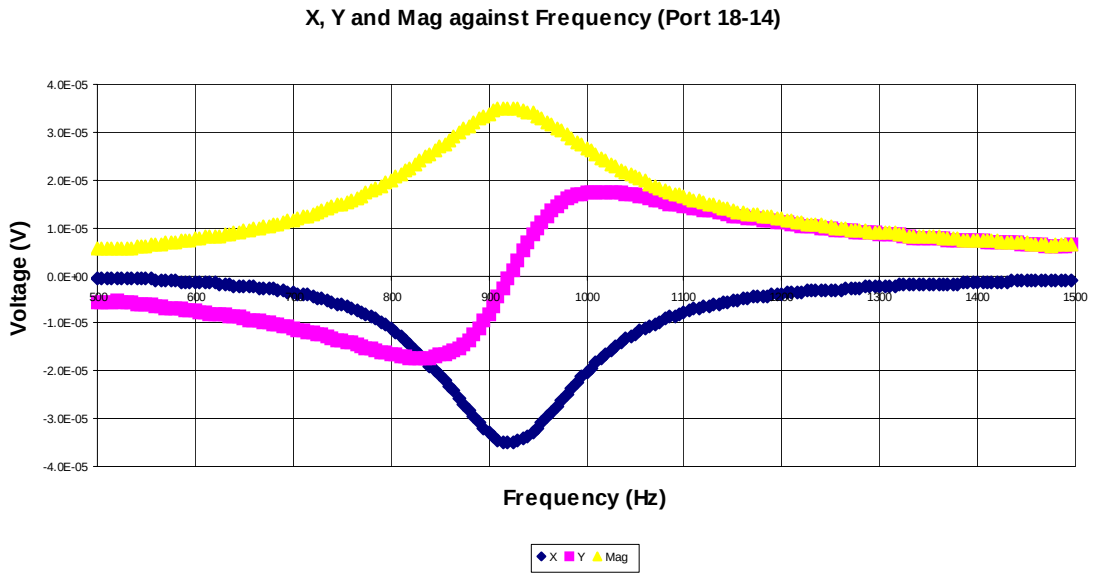

Fig.7.4. 3f detection for port 18-14

An up-converter output frequency is at the sum of the input and pump frequencies. So if the signal is to be at about 300 Hz, a filter at $300+900=2100$ Hz will be required for the implementation of an up-converter. The theoretical maximum gain possible is $\frac{2100}{300}=7\approx 17$ dB.

We will only use port 10 and mass 14 for the implementation of the parametric amplifier. The subsequent device parameters are also obtained with this configuration in mind.

7.2.3 Vacuum chamber testing

To increase the amount of capacitance change at resonance, the rest of the testing are done in a low pressure environment. A MMR vacuum chamber (Fig. 7.5) pumped till about 6 mTorr, is used.

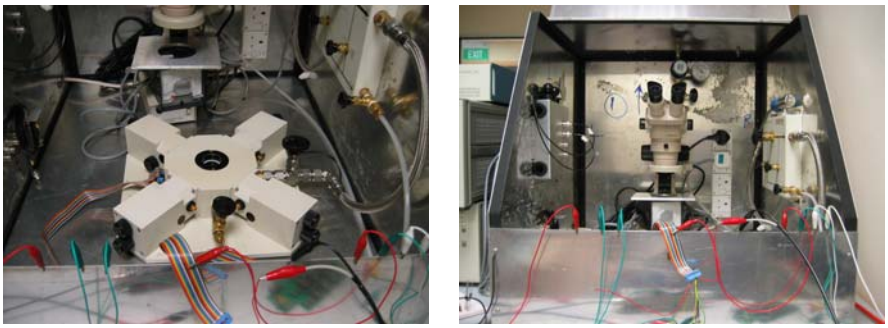

Fig. 7.5. Pictures of MMR Vacuum Probe station

The resonant frequency is again obtained at this pressure. The resonance of port 10-14 is shown in Fig. 7.6.

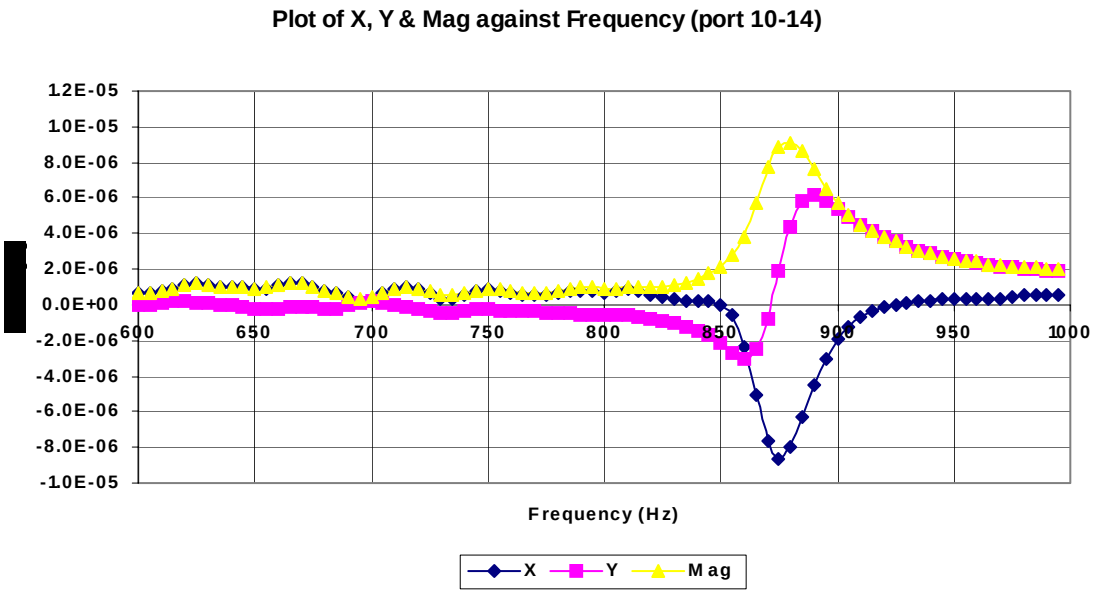

Fig. 7.6a. Frequency response from 600-1000 Hz

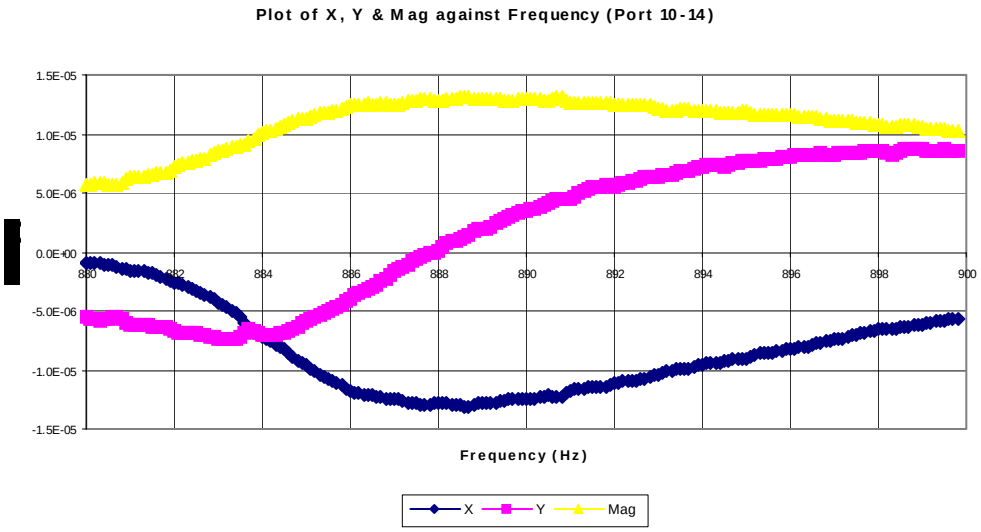

Fig. 7.6b Frequency response at 880-900 Hz

Comparing Fig. 7.6a to Fig. 7.3, the resonance peak is much sharper since it is done in vacuum. Fig. 7.6b shows the frequency response as the scanning is done at higher resolution (0.1 Hz). From Fig. 7.6b, we can see that the resonance frequency is about 888 Hz.

7.3. Device Parameters

7.3.1 C_p-D curve

The Capacitance-Dissipation curve is useful in determining various characteristics of the device. It can show the response of the device to potential applied as well as the pull-in voltage which the device fails. This can be obtained from the HP Impedance Analyzer 4194A.

For a device which is functioning well, it should show a quadratic relationship between capacitance and applied voltage (due to the fact that the resultant force on the plates is dependent on V^2). Naturally, the curve should then be symmetrical. The static capacitance C_0 can also be obtained here. The C-D curve is for the device is shown in Fig. 7.7.

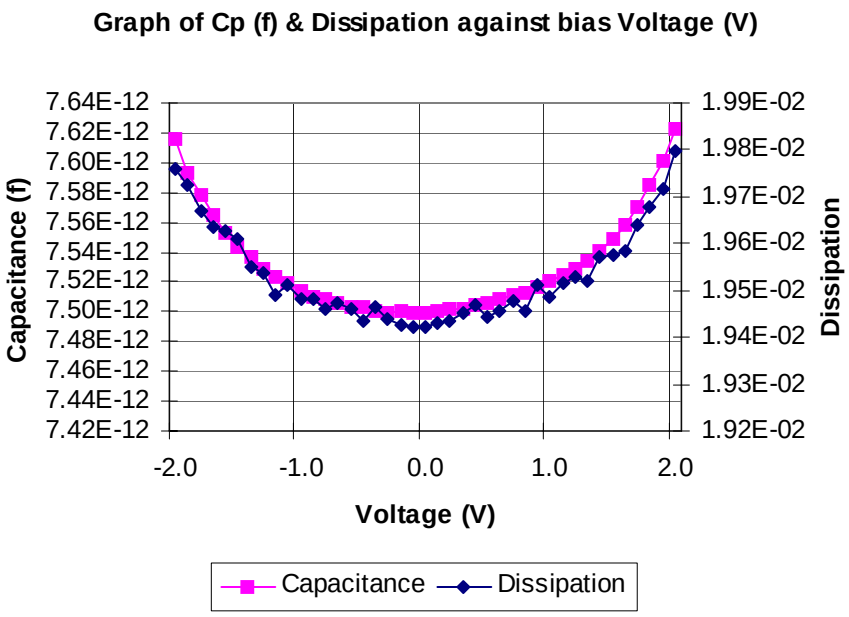

Fig. 7.7. C-V curve for port 10-14

From previous experience, the device snaps (the mass touches the plates) at between 2-3 V. We then limit the C-D measurement to stop at ± 2 V. As seen from Fig. 7.7, the C-D curve shows good symmetry, demonstrating good electrostatic characteristic of the device. Non-symmetrical curves often means that there are residue charges static on the plates, which is often the cause of unexpected results during further testing. From the curve, we can also approximate C_0 = 7.5 pf.

7.3.2 Internal resistance, R_c

The means of obtaining the internal resistance of the device has been explored in Chapter 5. Through the application of a high frequency voltage to the device, the Impedance Analyzer is able to do measure resistances. For this case, the real and imaginary components of impedance are obtained for various DC bias voltages. The resulting curve is shown in Fig. 7.8.

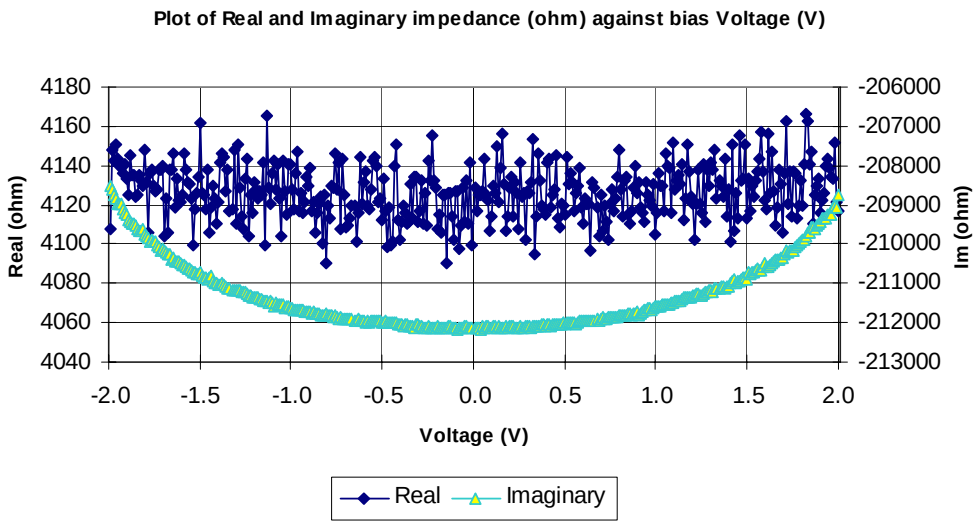

Fig. 7.8. Real and Imaginary impedance values

In fact, Fig. 7.7 and Fig. 7.8 shows two sides of the same coin. The Impedance Analyzer performs the same operation to obtain both plots. It is the post-processing done internally which results in different curves. For example, the imaginary impedance values obtained here can be extracted from the C-D curve if you know what frequency the analyzer sent into the device (since we know that $\mathrm{Im} = \frac{1}{jwC}$). As such, since the imaginary impedance (mostly capacitance in this case) is very much higher than the real impedance (two orders of magnitude higher), the plot still shows a quadratic relation between the imaginary values and the applied bias.

Part of the reason why the real values shows high scattering is because its values are small when compared to the imaginary. The internal resistance of the device should not be affected by the bias applied to the device. Therefore, taking the average is a reasonable way to extract the resistance. For the device, we can approximate the resistive value of the device, R_c = 4.12 kΩ.

7.3.3 Coefficients, γ_n

With the various parameters obtained above, the next target is to find the coefficients γ_n as a function of the applied pump signal. As mentioned in Chapter 5, we would require some post processing on the sampled *i(t)* data. The applied AC voltage is varied on port 10 with port 18 grounded. The rest of the ports for the actuation and ground

are all grounded as well. The mass is attached to the current amplifier as shown in Fig. 7.9.

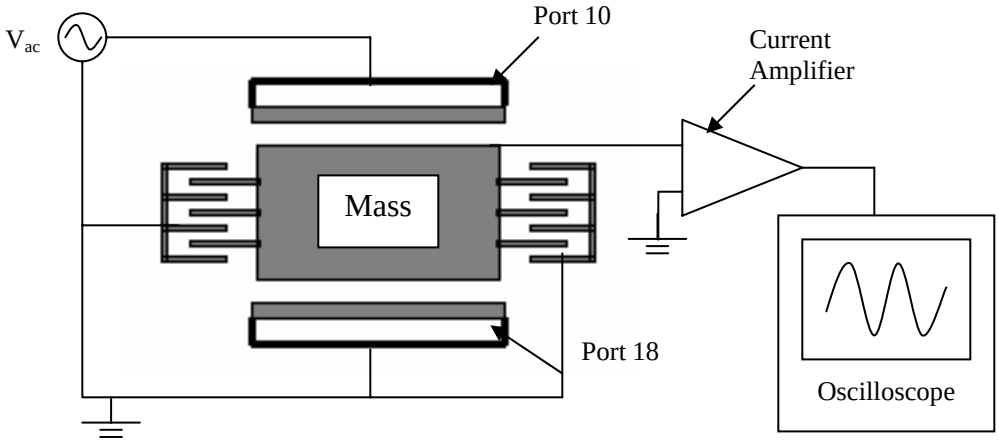

Fig. 7.9. Schematic of setup to measure γ_1

The output of the current amplifier is then fed into an oscilloscope. The output waveform is then recorded.

The applied AC was varied from 0.3 V to 1.0 V (peak values). The 1.0 V limit is chosen as a safety limit as resonance might result in the snap-in of the device. The current data was sampled at 100 kHz in the oscilloscope. The extraction procedure is carried out as described in the Chapter 5, section 5.5.

A summary of the extracted values is given in Table 7.2. The sampling rate from the oscilloscope was 100 kHz, with a total sampling time of about 0.1s.

Table 7.2: List of extracted γ_1 values

V_{ac} (Peak)	**γ_1**
0.3	0.0018
0.4	0.0022
0.5	0.0024
0.6	0.0030
0.7	0.0042
0.8	0.0054
0.9	0.0066
1.0	0.0078

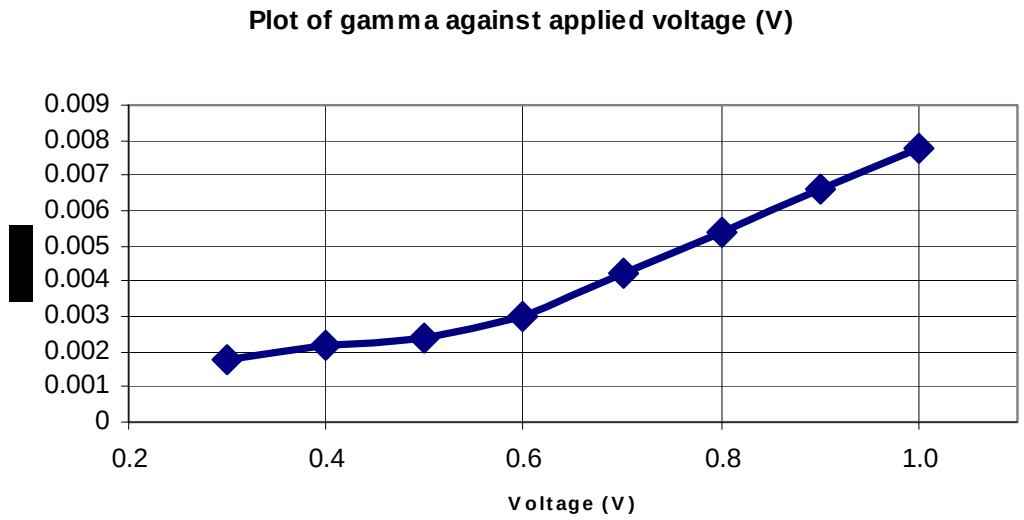

Fig. 7.10. Plot of extracted γ_1 variation with voltage

Fig. 7.10 shows the value of γ_1 increase as with applied actuation voltage, which is expected. The apparent linearity from 0.5–1.0 V might suggest that setting the limit at 1.0 V might be too conservative (since we are expecting a quadratic relation). For protection of the device however, we do not intend to push it too near its limit.

From the data, we see that the maximum γ_1 we can achieve is not very high, at around 0.008.

The next step is to design the filters required. The knowledge of the resonance frequency in section 7.2.3 has allowed the planning of the various bandpass filters required.

7.4. Filter Design

Table 7.3 shows the theoretical values obtained from the FilterPro^{TM} program required to achieve the filter characteristics. As exact matching of resistor values may not be possible, some slight deviations from the desired values are inevitable. Two filters are designed: one with the central frequency at 906 Hz, the other at 2.1 kHz. The passband bandwidths are both at about 200 Hz.

The input signal at about 300 Hz that is to be magnified will be from a function generator. As such, the source's internal impedance (R_g) is fixed at 50 Ω, the standard source impedance value for most instruments. Since the signal is from a function generator, it should not carry too much stray signals. The 300Hz filter is therefore

designed purely as a tuned circuit, since not much attenuation of other frequencies will be required.

Table 7.3: Theoretical and Practical values of resistors

		906 Hz		2.1 kHz		300 Hz	
		Theoretical	Practical	Theoretical	Practical	Theoretical	Practical
First stage	$\mathbf{R_1}$	162.0 k	160 k	73.2 k	72.63 k	536 k	535.4 k
	$\mathbf{R_2}$	162.0 k	160 k	73.2 k	72.63 k	536 k	535.4 k
	$\mathbf{R_Q}$	4.64 k	4.631k	1.82 k	2.0 k	49.9 k	49.9 k
Second stage	$\mathbf{R_1}$	191.0 k	192 k	78.7 k	78.92 k		
	$\mathbf{R_2}$	191.0 k	192 k	78.7 k	78.92 k		
	$\mathbf{R_Q}$	4.64 k	4.631 k	1.82 k	2.0 k		

With each biquad realizing a second order filter, we cascade several biquads in series to obtain either fourth order or sixth order filter depending on the roll-off attenuation required.

In our case, two fourth order filters using two stages each is designed. Each filter has a passband of about 200 Hz. The theoretical frequency responses for the two bandpass filters designed are shown in Fig. 7.11 and 7.12. Fig. 7.11 shows the theoretical result for the bandpass at 906 Hz, Fig. 7.12 shows bandpass at 2.1 kHz.

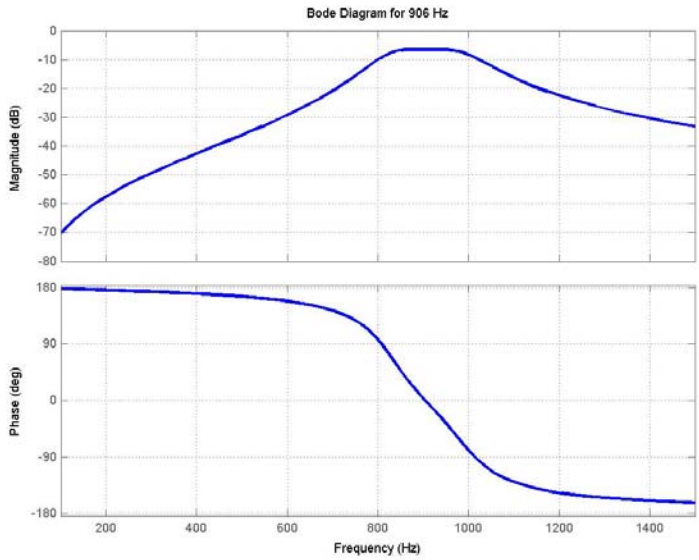

Fig. 7.11. Bode plot for bandpass centered at 906 Hz

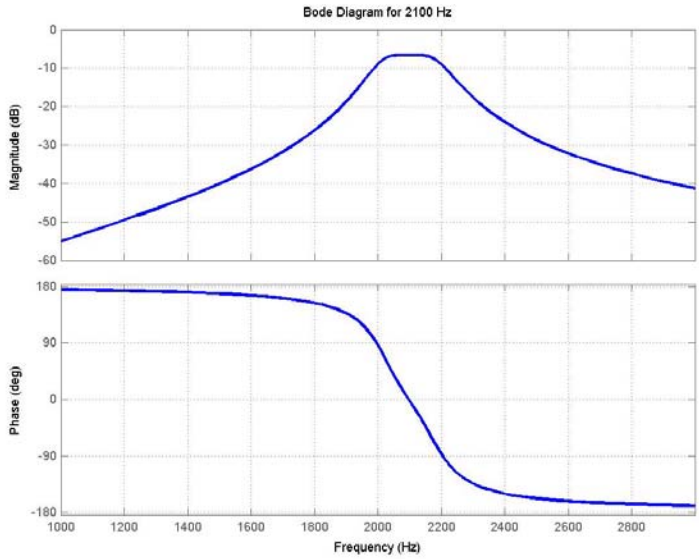

Fig. 7.12. Bode plot for bandpass at 2.1 kHz

7.4.1 Circuit Board design

A PCB board was designed for the filters so as to minimize possible sources of noise due to poor connections. Prior testing of the circuits on a breadboard is carried out before the final design. The final board with the various connections is shown in Fig. 7.13.

Capacitors of 0.1 farad are placed parallel between the power supply lines and the IC pins to smoothen out any possible power fluctuations from the source.

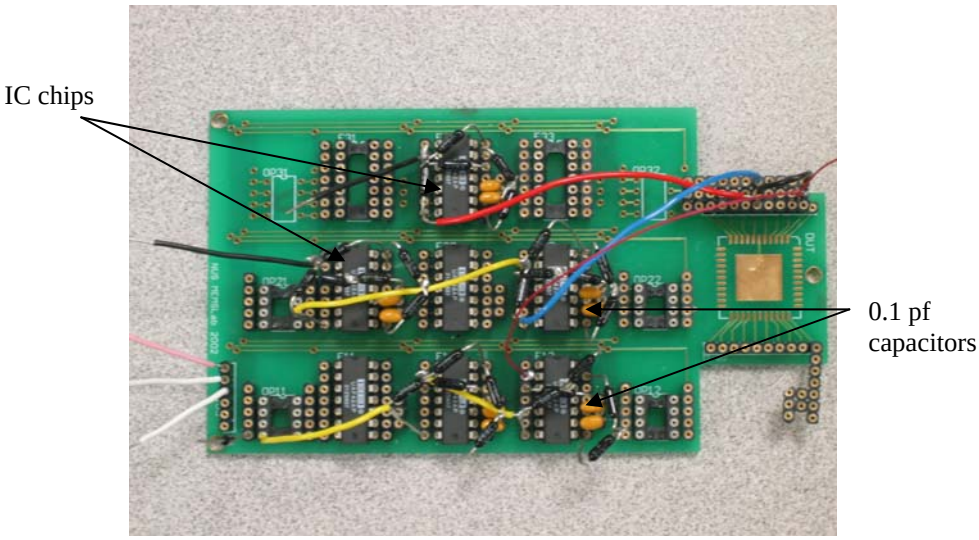

Fig. 7.13. Assembled filters on PCB

The gain-phase results for the filters implemented on the PCB are shown in Fig. 7.13 and Fig. 7.14. The gain-phase plots are obtained through the use of a HP 4194A Spectrum Analyser.

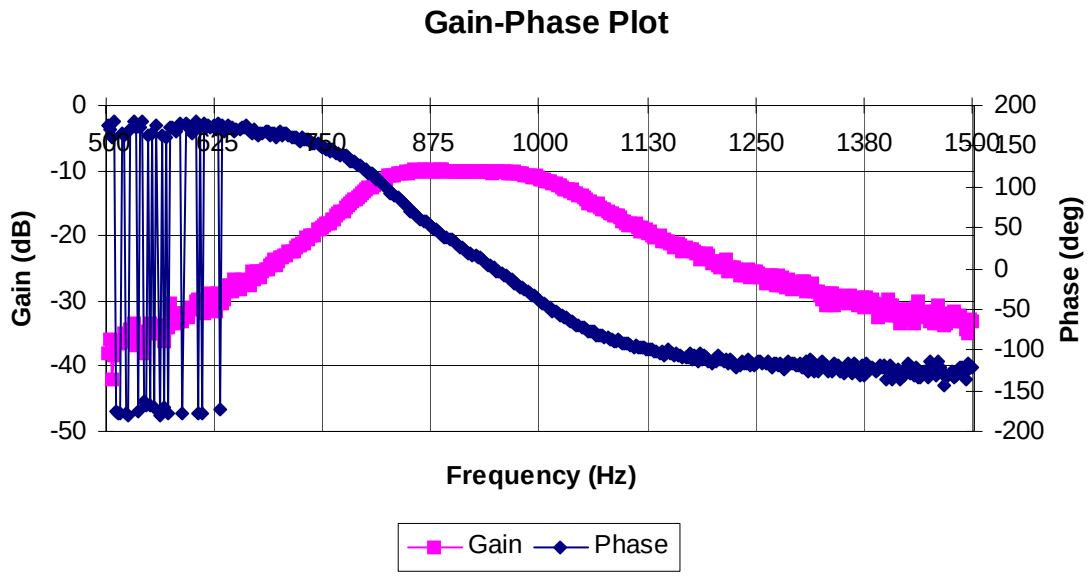

Fig. 7.14. Gain-phase for pass band at 906 Hz

At the passband, there is about -10dB of attenuation. The filter behaves exactly as designed. The attenuation at high frequencies is significant, with already 30 dB at 1.5 kHz.

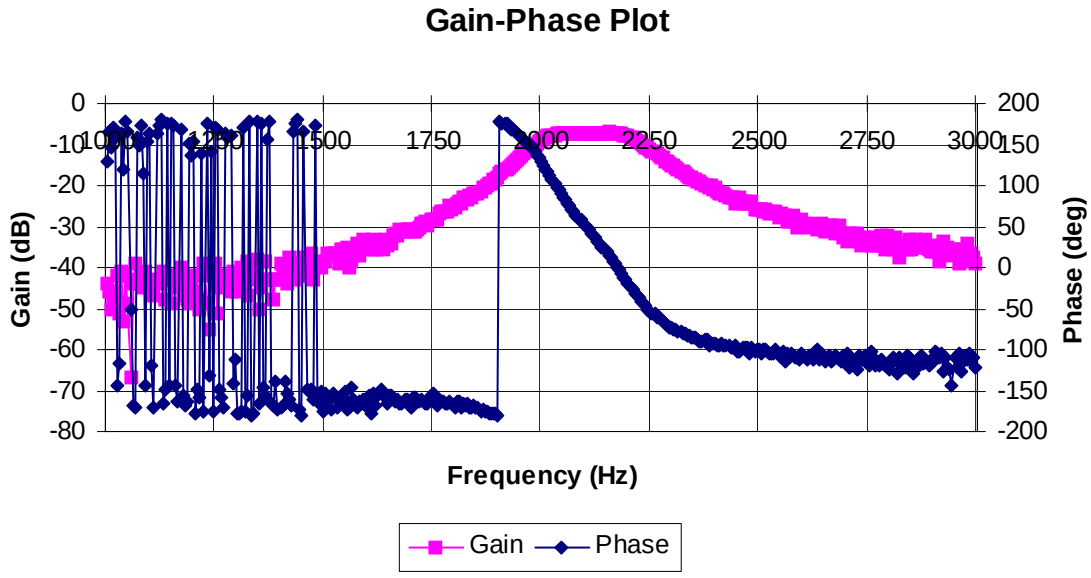

Fig. 7.15. Gain-phase for passband of 2.1 kHz

The passband attenuation in this case is about -7dB. The attenuation of lower frequencies is also of interest here (to cut-off the pump signal). At 1 kHz, the attenuation is also significant at about 40 dB.

7.5. Up-Converter Gain

With the foundation established, the next step is to incorporate everything to verify parametric amplification for an up-converter device. Initially, attempts were made to decouple the pump and signal by using the configuration shown in Fig. 7.16.

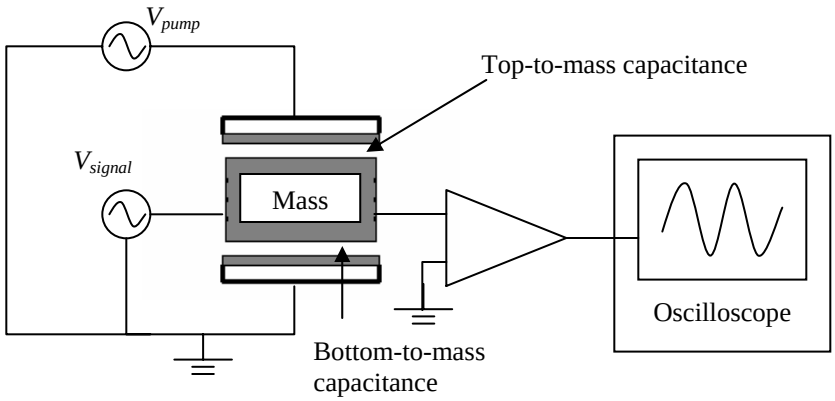

Fig. 7.16. Originally intended configuration

It was hoped that such a configuration would render the filters at the signal and pump frequencies unnecessary, since the pump resonates the 'top-to-mass' gap of the device, leaving the 'bottom-to-mass' gap for the mixing of charges when the signal voltage is applied. This will be analogous to parametric amplification done by Rugar et al [14] and Carr et al [13] where the use of optical detection removes the necessity for filters altogether. The implementation of different energy domains ensures that the signals at output are decoupled i.e. the actuation force is not picked up by the optical sensor.

However, attempts to detect signals using this configuration were unsuccessful. No mixing of signals was detected, and no output at 2.1 kHz was observed. The success of this configuration lies on the assumption that the signal can produce mixing due to capacitance change at the 'bottom-to-mass' gap *only*. In practice however, mixing should also occur at the 'top-to-mass' gap, since there is capacitance change there as well. Another possible reason is that by applying two different frequencies at two locations (one to the top plate and another to the mass), the resulting structure may not be resonating at

the frequency assumed, i.e. at 1.8 kHz. Thus the resulting mixing cannot be detected at 2.1 kHz.

An alternative and simpler method is then used. The setup of the experiment is shown in Fig. 7.17. The signal and pump sources are from a Yokogawa FG 300 Synthesized Function Generator. The detection can be either a Yokogawa DL1520 Digital Oscilloscope or a HP 89410A Vector Signal Analyzer (VSA), depending on the sensitivity required.

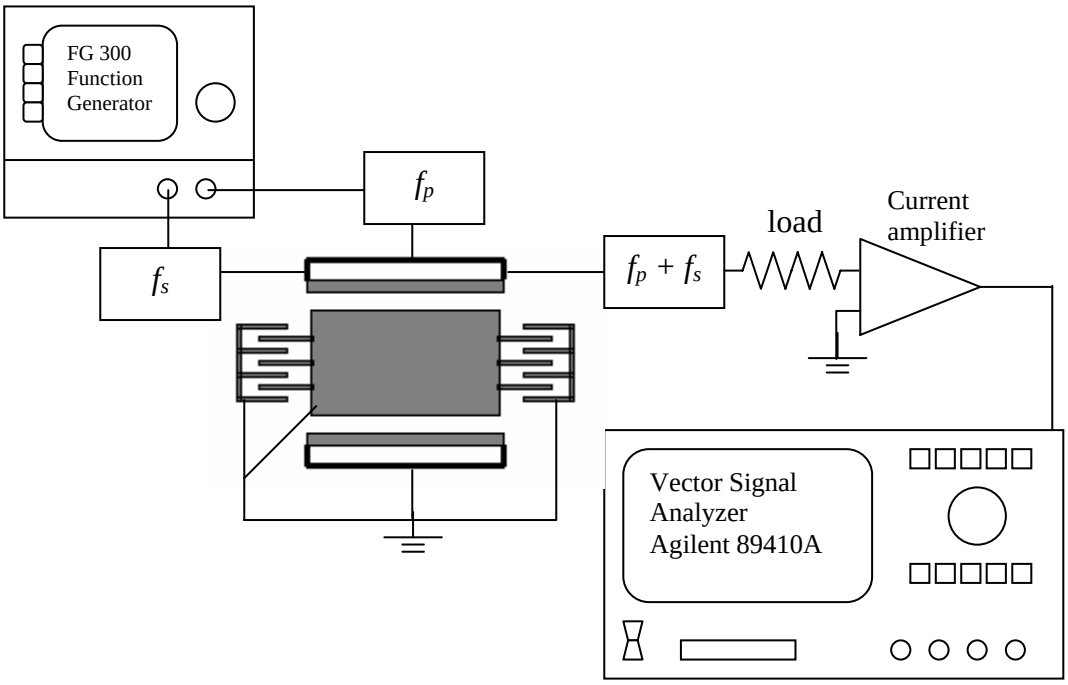

Fig. 7.17. Schematic of experimental setup

The signal and pump frequencies are supplied from the same function generator, with a fixed source impedance of 50 Ω. All the signals and outputs are tapped from port 10 of the package. The mass, actuating combs and port 18 are all grounded. To minimise problems and compensations required when using probe tips [30], output at the load is fed directly into a current amplifier before sending into the VSA. The only inconvenience in this case is that an additional step is required to compensate for the current gain. This is considered minor compared to compensating for the probe impedance when measuring potentials across high resistance (up to 1 MΩ in our case).

As a side note, it is found that the presence of the filters is imperative, as assumed by theory. Without any one of the filters (for example connecting the pump directly to port 10), no mixing of frequencies occurs and no output at 2.1 kHz is detected.

We first look the impedance characteristic of the device. From Chapter 3, it was derived that

$$R_{in} = \frac{\gamma^2}{w_1 w_3 C^2 R_{T3}} \qquad 3.28$$

$$R_{out} = \frac{\gamma^2}{w_1 w_3 C^2 R_{T1}} \qquad 3.29$$

The effective output impedance of the device depends on the input source impedance, which in our case does not change much since the source impedance is fixed at 50 Ω. It is simply then

$$R_{T1} \approx R_g + R_c$$

$$\approx 50 + 4120 = 4170\ \Omega$$

The tabulated values of output impedance for the various γ_1 values are shown in Table 7.4.

Table 7.4: Output impedance for different pump voltage

V_{ac} (V)	γ_1	R_{out} (Ω)
0.3	0.0018	536,000
0.4	0.0022	801,000
0.5	0.0024	954,000
0.6	0.0030	1,490,000
0.7	0.0042	2,921,000
0.8	0.0054	4,830,000
0.9	0.0066	7,215,000
1.0	0.0078	10,077,000

The operating frequencies and C_0 are those obtained from the device.

$w_1 = 2\pi f = 2\pi \times 324Hz = 2034.7$ rad/s

$w_3 = 2\pi \times 888Hz = 13188$ rad/s

$C_0 = 7.5\,\text{pf}$

By varying the pump voltage, the effective output impedance of the device can be changed from 500 kΩ to 10 MΩ. This is a very wide range of impedance change, for an input change of only 0.3-1.0 V.

On the other hand, the effective input impedance of the device depends on R_{T3}, which depends largely on the load. As an example of the characteristic, we look at the variation for the case in which $V_{ac} = 1V$, and varying the load. The other parameters are as above. The tabulated values for selected load resistances are shown in Table 7.5.

Table 7.5: Input impedances for fixed pump voltage

Load (Ω)	γ_1	R_{T3} (Ω)	R_{in} (Ω)
50	0.0078	4,170	9,666,000
511	0.0078	4,631	8,704,000
1000	0.0078	5,120	7,873,000
4990	0.0078	9,110	4,425,000
10000	0.0078	14,120	2,855,000
49900	0.0078	54,020	746,000
150000	0.0078	154,120	262,000
249000	0.0078	253,120	159,000
511000	0.0078	515,120	78,000
1000000	0.0078	1,004,120	40,000

The resistance values chosen are those physically available and attempted to cover as wide range as possible.

The implication of this variation of effective output and input impedance of the device is that the parametric amplifier can be made to act as a buffer between a low impedance source and a high impedance load or vice versa. The aim then is to maximize power transfer even though the system itself has mismatch source and load impedance values. This is achieved by varying the amount of pump signal and, if possible, varying the value of C_0 through the application of a DC bias to the device.

To verify the excitation involved, only the pump signal at 888 Hz is turned on and the output current is measured. As expected, only a current at 1776 Hz (*2w*) is detected (Fig. 7.18). There is another smaller signal of 2664 Hz (*3w*) that is due to the non-linear excitation as mentioned in Chapter 2.

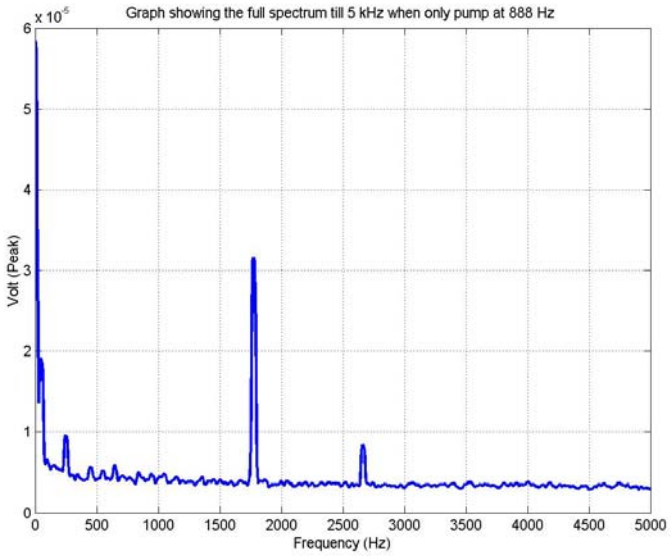

Fig. 7.18. Plot when only pump signal is sent in

Next, both pump (888 Hz) and signal (324 Hz) are sent into the device. The results shown next in Fig. 7.19 is a sample done for a load at 4.99 kΩ. To demonstrate that the output signal is truly dependent on the frequencies of the two sources and not some noise or arbitrary signal present, the signal is changed to 350 Hz. What can be observed in the VSA is a shift in the various signals present. This change is shown in the Fig. 7.19 (in red). All the various signals are permutations of the pump and signal frequencies. Their relations are shown as well. The arrows shows the shift observed in the signal.

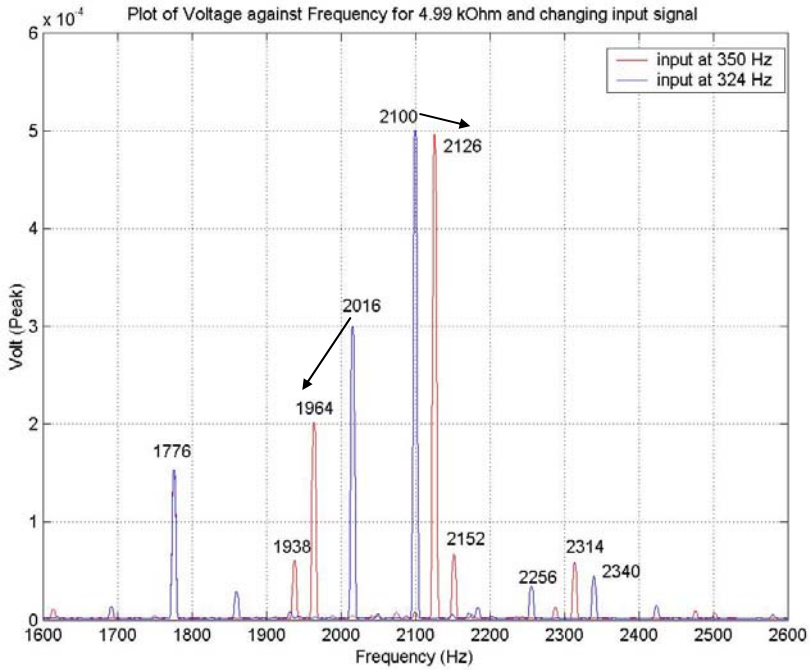

Fig. 7.19. Plot showing the shift in frequencies

The various frequencies' configuration (in blue) apparent are shown below:

$2f_p + f_s = 2100\,\text{Hz}$

$3f_p - 2f_s = 2016\,\text{Hz}$

$2f_p - f_s = 2340\,\text{Hz}$

$4f_p + -4f_s = 2256\,\text{Hz}$

As a digression, from looking at the shift, one might be tempted to question the outcome if the two largest peaks are brought together i.e. the input frequency required to make $2f_p + f_s = 3f_p - 2f_s$. This works out to $f_s = 296\,\text{Hz}$, resulting in an output at 2072 Hz as shown in Fig. 7.20 (in red).

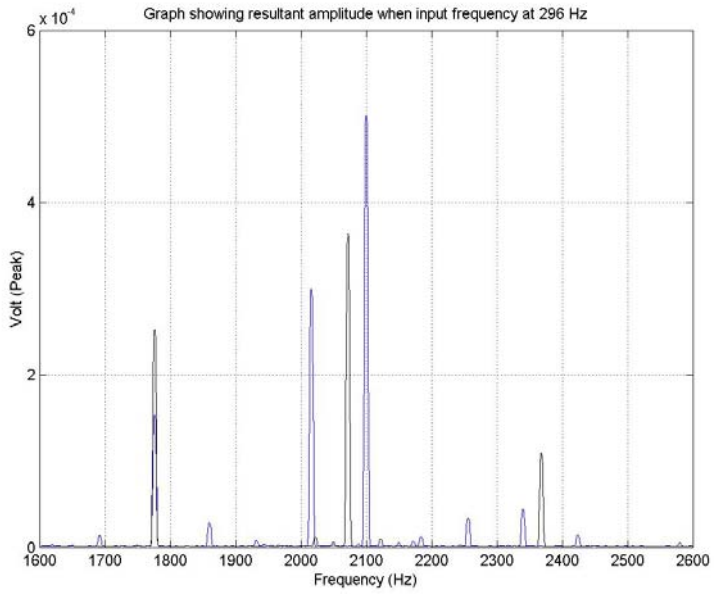

Fig. 7.20. Plot showing output for 296 Hz

The converged signal shows a signal strength which is in between that of $3f_p - 2f_s$ and $2f_p + f_s$ alone. No analysis has been done at this present moment to explain why the signal at 296Hz is not the sum of the two converged signals. One aspect of the signals not shown on the plots is their actual phases. One possible reason for the loss in signal strength is that $3f_p - 2f_s$ and $2f_p + f_s$ are not coherent, i.e. there is a phase

difference between them. This special situation aside, the phase of the output signal is inconsequential since we are only interested in the magnitude gain of the signals involved.

Having demonstrated that the signals are truly the resultant of mixing of signals within the MEMS device, the approach is applied to non-degenerate amplification. Two aspects will be verified: the relation between gain and load, R_l and the relation between gain and γ_1.

7.5.1 Gain-Load & Gain-γ_1 Relationships

To obtain these two relationships, two terms are varied: the pump voltage, V_{pump} and the load, R_l. Varying V_{pump} effectively changes the γ_1 based on the extracted values obtained earlier. However, additional compensation for the insertion loss of the filter has to be taken into account. For example, input at 888 Hz of 5.0 Vpp has a loss of about 9 dBV, which results in the actual voltage being about 1.0 V_{peak}.

The pump voltage is varied from 5.0 Vpp to 1.5 Vpp in steps of 0.5 Vpp. This practically covers the range of γ_1 that had been extracted previously. The corresponding γ_1's are estimated through a linear interpolation from the results obtained.

The concept of gain might be subjective. Certain works define gain in forms like the increase in signal strength after subjecting the system to the pump voltage [13]. This method of defining gain can be confusing but in general yields much higher gain. Carr et al [13] quoted gains of about 30 dB. This is due to the fact that without the pump, the output frequency signal is very small, practically near the noise floor. The application of the pump signal results in the output frequency becoming prominent, thus the huge gain calculated.

However, in our case, the gain is defined as a measurement of power gain over the available power from the signal, as per derived in Chapter 3. This is because our focus is on the amount of power transfer from the input to the output frequency.

Table 7.6. summarizes the obtained values. All the values are in dB.

Table 7.6: List of gain obtained in dB

V_{pp} / Ω	1.5	2.0	2.5	3.0	3.5	4.0	4.5	5.0
	γ_1=0.19e^{-2}	0.23e^{-2}	0.26e^{-2}	0.31e^{-2}	0.48e^{-2}	0.61e^{-2}	0.74e^{-2}	0.78e^{-2}
1000	-114.5	-107.2	-102.5	-101.2	-90.8	-125.5	-129.2	-126.5
4990	-101.2	-92.9	-87.3	-84.5	-88.2	-108.5	-112.2	-109.3
10000	-95.3	-87.1	-81.8	-79.0	-86.8	-103.0	-106.2	-103.4
49900	-109.3	-101.3	-96.2	-93.1	-91.1	-89.0	-92.3	-89.9
66500	-111.9	-103.9	-98.9	-95.7	-93.7	-91.6	-89.9	-87.8
107000	-116.2	-108.0	-102.9	-100.0	-97.7	-96.3	-94.3	-92.6
150000	-118.7	-109.9	-104.0	-100.3	-97.2	-94.9	-92.7	-91.3
221000	-121.7	-113.2	-107.5	-103.6	-101.4	-99.4	-96.9	-95.7
249000	-122.8	-114.0	-108.6	-104.7	-102.6	-100.5	-98.3	-96.9
511000	-129.1	-120.5	-114.6	-111.0	-108.5	-106.4	-104.5	-103.0
1000000	-134.1	-126.3	-120.4	-116.5	-114.1	-112.0	-109.8	-108.3

A comparison between the theoretical and experimental results for the case of 5.0 Vpp is shown below in Fig. 7.21

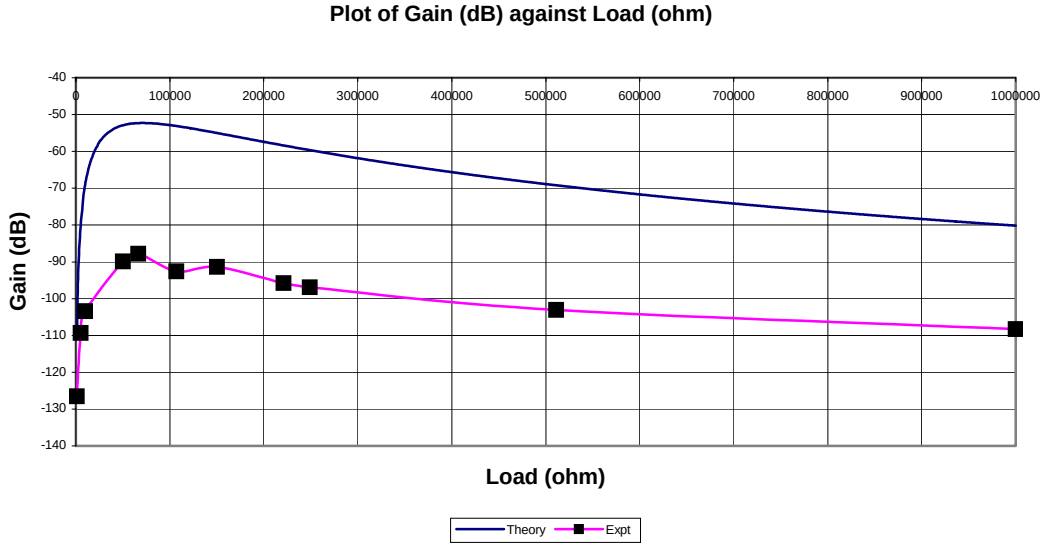

Fig. 7.21. Plot comparing theoretical and experimental values for 5.0 Vpp.

There are a couple of issues here. Firstly, the effect of a device resistance of 4.12 kΩ is now apparent. At such high resistances, too much power is lost within the device. Moreover, the amount of capacitance variation (γ_1) is too low, with a comfortable value at a maximum of 0.0078. Both of these factors contribute to the amount of theoretical gain possible, about –50 dB in this case. As a comparison, Raskin et al [12] used a huge

membrane which has internal losses of only 140 Ω and is capable of achieving $\gamma_1 = 0.2$. In contrast, they were able to achieve gain of about 9dB.

Comparing our experimental and theoretical results then, there is consistently about 40-50 dB differences in gain, even for other pump voltages. Besides the fact that there may be other losses unaccounted for in the circuit, the nature of the filters used is a contributory factor as well. The use of active filters instead of passive filters solved the issue of having to design different filters: two for every point on the table (one for the signal and the other for the output). That would have constituted about 176 filter designs simply to match the filter characteristics needed.

However, active filters introduced another issue by itself. Solid state electronic devices do not have the characteristic of achieving maximum *power* transfer. Instead, it achieves maximum *voltage* transfer [31]. This is most likely the reason for the amount of losses within the circuitry.

Nevertheless, the resistive value that maximizes gain can be approximated from the theoretical values, given the limited number of resistor points available. A comparison is shown in Fig. 7.22.

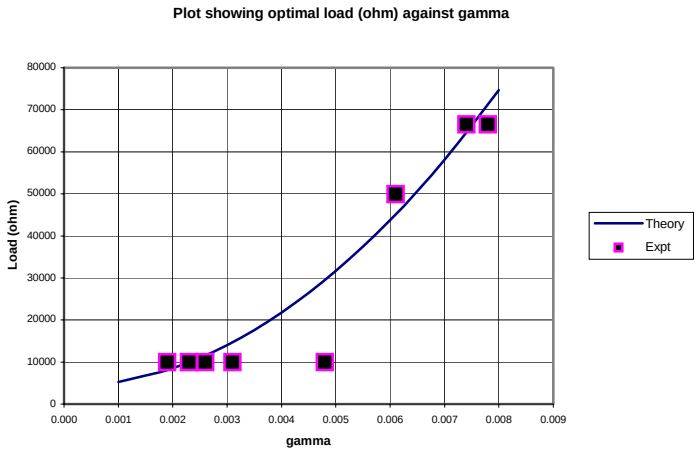

Fig. 7.22. Predicted and experimental optimal gain

Fig. 7.21 shows a characteristic which is unique for parametric amplifiers, where the impedance that results in maximum power transfer can be varied by another signal. In this case, some form of tuning is achieved by varying the pump voltage. Fig. 7.21 shows that the theory predicts the optimal load very well, except for the case where $\gamma_1 = 0.0048$.

That is because the resolution of the load resistances used is not high: there is no resistance used between 49.9 kΩ and 10 kΩ. Either of these values would not have fitted the curve.

The dependence of gain on γ_1 is shown in Fig. 7.23. It is simply plotted for various constant loads.

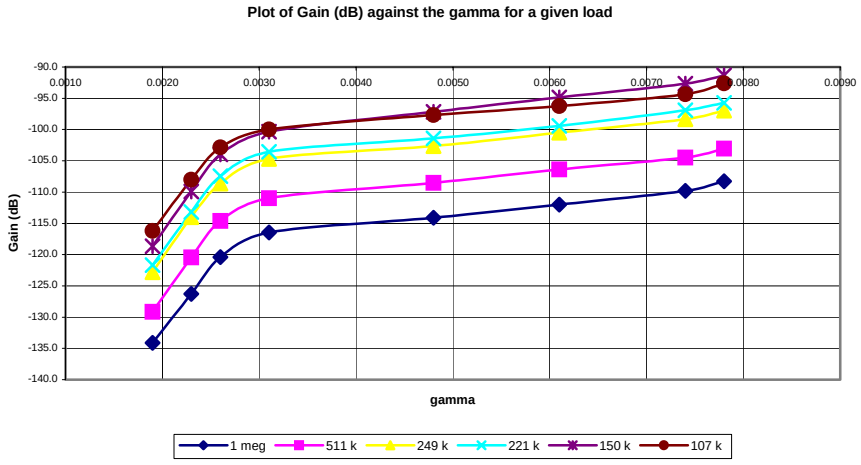

Fig. 7.23. Gain dependence on γ_1

As expected, the gain for a given load increases as γ_1 is increased. Though at loads lower than 107 kΩ, the relation of the gain starts to become erratic. At the present moment, the only plausible reason is because of the use of active filters instead of passive ones.

CHAPTER 8: Conclusion

As with all systems, the implementation of a parametric amplification system is not straightforward. Several issues and unknowns have to be resolved. As a first step towards understanding the system, the theoretical derivation is adapted to suit MEMS devices. With the theoretical background established, the necessary ingredients to implement a parametric amplifier become clearer.

Firstly, the device has to be appropriate. The resonance frequency and capacitance change has to be high, with low internal resistance and parasitic capacitance. The last two factors are not easily designed, being a function of process and careful placement of electronics. However, the first two factors are easier to control through the design of the structure. In this project, no optimized device was fabricated since the aim is to verify the possibility of parametric dependence for the output signal. With the numerous devices available in our laboratory, a BARS gyroscope was the device of choice due to its high resonance frequency (compared to the other devices available) as well as its stable capacitance variation.

Parametric amplification requires the various signals to be contained within their individual loops, with mixing only occurring within the device itself. To achieve this, filters were designed and implemented for each of the loops. This is necessary since we are working totally in the electrical domain, unlike other works where different energy domains were used for actuation and detection. An initial configuration for the device was proposed that might have removed the need for filters. However, that configuration did not achieve the objective and a simplified version was used instead.

As there is no direct means of measuring the amount of capacitance change (γ_n) in the device during actuation, a method is proposed to extract this value from the current signals. This parameter is important in the analysis of parametric amplification.

In the process of the implementation and characterization of the system, two methodologies are proposed. Firstly, a *3f* detection scheme is proposed which allows the detection of one-port devices previously unattainable by other methods. The influence of parasitic capacitance makes the detection of resonance difficult. Methods such as EAM and *2f* detection normally used to circumvent this problem, are only applicable to 2-port

devices. This *3f* method removes that restriction. Analysis and demonstration of the method is shown and it permitted the detection of resonance effectively.

A means of obtaining the equivalent electrical model of mechanical systems is proposed through the use of Bond Graphs. Such a scheme might be useful in extracting mechanical parameters from the analysis of the electrical signals. Such a method had already been demonstrated for single degree-of-freedom systems. What is proposed here is a way to extend that capability to higher DOFs.

Finally, the cumulative work are all integrated into the analysis and test of a parametric up-converter. The gain of the system is shown to be dependent on both γ_1 and load resistance, as predicted by theory. Though more losses within the circuit were measured than predicted, the general response of the system agreed with theory, especially the prediction of the load that gives optimal gain.

8.1. Future work

The interest in parametric amplification lies in its theoretical capability to achieve low-noise amplification. As such, noise analysis would be a very interesting aspect. Active filters cannot be used in this case, since the introduction of transistors introduces more noise. The implementation of the system has to be well planned as its load influences the filter characteristic of passive filters. A complete experimental programme to analyze and compare the noise figure of such parametric amplification at high temperatures with transistor based circuitry is suggested.

In order to fully exploit the gain of the amplification, the device that is being used should be optimized for high frequency resonance as well as large capacitance change.

It may also be interesting to explore alternative forms of parametric amplification configurations, for example the degenerate amplifier.

REFERENCES

1. J.M. Manley and H. E. Rowe, "*Some general properties of nonlinear elements – Part1: General energy relations*," Proc. of the IRE, pp.904-914, July 1956
2. H. E. Rowe, "*Some general properties of nonlinear elements—Part 2: Small signal theory*," Proc. of the IRE, pp.850-860, May 1958
3. Uenohara, M., and Bakanowski, A.E, "*Low-noise Parametric Amplifier Using Germanium p-n Junction Diode at 6 kmc*", Proc. IRE, vol. 47, pp. 2113-2114, December 1959
4. Michel Marhic, Frank Yang, Min-Chen Ho & Leonid G. Kazovsky, "*High Non-linearity Fiber Optical Parametric Amplifier with Periodic Dispersion Compensation*", Journal of Lightwave Tech, Feb 1999, Vol.17, no.2, 210-215
5. M.L.Bortz, M.A. Arbore & M.M. Fejer, "*Quasi-phase-matched optical parametric amplification and oscillation in periodically poled $LiNbO_3$ waveguides*", Optics Letters, Jan 1 1995, vol.20, no.1
6. Nyquist, H, "*Thermal agitation of electric charge in conductors"*, Physical Review, vol.32, pp.110-113, July 1928
7. J. Engberg & T. Larsen, Noise Theory of Linear and Nonlinear Circuits, John Wiley & Sons, 1995
8. Boris A. Kalinkos, Nikolai G. Kovshikov, Mikhail P.Kostylev, "*Parametric Frequency Conversion with Amplification of a Weak Spin Wave in a Ferrite Film*", IEEE. Trans. On Magnetics, Vol.34 P. 1393-1395 (1998)
9. Per. K. Rekdal & Bo-Sture K. Skagerstam, "*Quantum Dynamics of Non-Degenerate Parametric Amplification*", Physica Scripta. Vol.61, 296-306, 2000

10. B. Yurke, M.L. Roukes, R. Movshovich and A.N. Pargellis, "*A low-noise series-array Josephson junction parametric amplifier*", Applied Phys. Lett. 69 (20), Nov 1996

11. A.Dana, F Ho & Y. Yamamoto, "*Mechanical parametric amplification in piezoresistive gallium arsenide microcantilevers*", Applied Phys. Lett. 72 (10), March 1998

12. Jean-Pierre Raskin, Andrew R. Brown, Butrus T. Khuri_Yakub & Gabriel M. Rebeiz, "*A Novel Parametric-Effect MEMs Amplifier*," JMEMs, Vol.9, No.4, Dec 2000

13. Dustin Carr, Stephane Evoy, Lidija Sekaric, H.G. Craighead and J.M. Parpia, "*Parametric amplification in a torsional microresonator*", Appl. Phys. Lett. 77 (10), Sept 2000

14. D. Rugar & P. Grutter, "*Mechanical Parametric Amplifier and Thermomechanical Noise Squeezing*", Physical Rev Lett. Vol.67, no.6 Aug 1991

15. A. Olkhovets, D Carr, J.M.Parpia & H.G. Craighead "*Parametric amplification in nanomechanical resonators*", IEEE MEMS-2001 proceedings**,** January 2001

16. M. Zalalutdinov, A. Zehnder, A. Olkhovets, S. Turner, L. Sekaric, B. Ilic, D. Czaplewski, J. M. Parpia and H. G. Craighead, "*Auto-Parametric Optical Drive For Micromechanical Oscillators*", Appl. Phys. Lett. 2000

17. Chan Mei Lin, *Dynamic and Static Characterization of Microfabricated Resonating Structures*, Masters Thesis, National University of Singapore, 2002

18. J. Cao & C.T.C Nguyen, "*Drive Amplitude Dependence of Micromechanical Resonator Series Motional Resistance*", Dig. Of Tech.Papers, 10th Int. Conf. On Solid-State Sensors and Actuators, Jun 1999, pp. 1826-1829

19. William Tang, *Electrostatic Comb Drive for Resonant Sensor and Actuator Applications*, Phd Thesis, University of California at Berkeley

20. L Blackwell, K Kotzebue, *Semiconductor-Diode Parametric Amplifiers*, Prentice-Hall

21. Karnopp, Margolis, Rosenberg, *System Dynamics: A Unified Approach*, Wiley-InterScience Publication, 1990

22. C.T. Nyugen, Ph.D. Dissertation, 1994, UC Berkeley

23. Clark T.C Nguyen, "*Micromechanical filters for miniaturized low-power communications*", Proc. Of SPIE: Smart Structures and Materials, 1999

24. Kendall L. Su., *Analog Filters*, Chapman & Hall, 1996

25. Simon Haykin, *Modern Filt*ers, Macmillan, 1989

26. V.J. Logeeswaran, M.L. Chan, E.H. Tay, F.S.Chau & Y.C. Liang, "*A 2f method for the measurement of resonant frequency and Q-factor of micromechanical transducers*", Proc. SPIE Vol. 4755, DTIP 2002, Cannes pp.584-593

27. Chua Bee Lee, "ADA Framwork and its application to the development of MEMs devices," M.Eng. Thesis, National University of Singapore, 2001

28. J C Decroly, L Laurent, J C Lienard, G Marechal & J Vorobeitchik, *Parametric Amplifiers*, Macmillan, 1973

29. Douglas C. Smith, *High Frequency Measurements and Noise in Electronic Circuits*, Van Nostrand Reinhold, 1993

30. Dennis Bohn, *Unity Gain & Impedance Matching: Strange Bedfellows*, Rane Corporation, RaneNote 124

31. http://www.protel.com

32. http://www.ti.com

33. Burr-Brown® Application Bulletin (Filter Design Program for the UAF42 Universal Active Filter)

APPENDIX A

Bond Graphs

Glossary of Terms:

- Ports: connections between subsystems which allow power to flow between them
- Multiports: subsystems with one or more ports

Concepts:

- All power variables are either *effort e(t)* or *flow f(t)*
- Energy variables *momentum p(t)* and *displacement q(t)*
- $$p(t) = \int e(t)dt = p_0 + \int_{t_0}^{t} e(t)dt$$
  $$q(t) = \int f(t)dt = q_0 + \int_{t_0}^{t} f(t)dt$$
- **Efforts** are placed *above* or to the *left* of port lines
- **Flows** are placed *below* or to the *right* of port lines
- *Half arrow* indicates the direction of **power** flow at any instant of time
- *Full arrow* indicates an **active bond**, or a signal flow at very low or no power
- *Causal stroke*: short, perpendicular line which indicates direction of the **effort** signal
- Effort and flow signal flow in **opposite** directions

Basic Component Models:

1-port elements

- Resistance--------- *R*
- Capacitor---------- *C*
- Inertia---------- *I*
- Effort source------ S_e

- Flow source------- S_f

2-port elements

- Transformer------- *TR*
    - Modulated transformer--- *MTR*
- Gyrator----------*GR*
    - Modulated gyrator-------- *MGR*

3-port elements

- Flow junction, *0*-junction or common effort junction
- Effort junction, *1*-junction or common flow junction